TEST RESULTS FOR AN OPEN-END SQUEEZE FILM DAMPER WITH A HIGH VISCOSITY OIL

Aquiles Lopez

Dr. San Andres

May 1995

TRC-SFD-1-95

Texas A&M University
Mechanical Engineering Department

Test Results for an Open-End Squeeze Film Damper with a High Viscosity Oil

by

Aquiles Lopez
undergraduate research assistant

A Research Progress Report
to the
Turbomachinery Research Consortium

May 1995

TRC Project:
Experimental and Analytical Study of the Non-Linear Response of Squeeze Film Damper Supported Rotors.
Principal Investigator: Dr. Luis San Andres, Associate Professor

Table of Contents

ABSTRACT

Dynamic pressures and film force measurements for a fully submerged, open end squeeze film damper (SFD) are presented for increasing whirl frequencies and supply pressures. The damper journal describes centered circular orbits. The orbit radius varies inversely with fluid viscosity and whirl frequency. The peak–to–peak dynamic pressures increase linearly with lubricant viscosity. A combination of gaseous and vapor cavitation was observed throughout the different test conditions. As viscosity increased, the extent of the cavitation zone also increased. The radial and tangential fluid film forces (and damping coefficients) present a linear relationship with viscosity and increase with increases in whirl frequency.

Increments in the supply pressure to the damper also increased the peak–to–peak pressures and reduced the extent of the cavitation zone. External pressurization had little effect on the radial force (and cross–coupled damping coefficient), but it increased significantly the tangential force (and direct damping coefficient). Comparison of the test results with theoretical predictions is acceptable. The differences may be attributed to the test journal not being perfectly centered within the damper bearing housing.

INTRODUCTION

Lighter and more flexible rotating machinery have been developed to satisfy the demands for higher performances. Unlike their predecessors, sturdy and massive machines, these engines are known to be very sensitive to vibration. In other words, current high-speed machines are not able to achieve maximum or desired design performance because of the onset of high undesirable levels of vibration.

One of the most effective ways of attenuating high vibration levels is through the implementation of a squeeze film damper on the bearing supports. Wherever damping and stability are necessary, squeeze film dampers (SFDs) prove themselves ideal. Squeeze film dampers have the ability of attenuating the amplitude of rotor vibrations and decreasing the forces transmitted to structural components. SFDs are mostly used as retrofits for unstable systems at full operating conditions. However, SFDs have also been implemented in the design and manufacturing of many turbomachines. For instance, modern aircraft jet engines operate on rolling-element bearings because of their long life and low power consumption. Since these bearings provide negligible damping to the rotor, SFDs are implemented. Another application of squeeze film dampers occurs in high pressure compressors. Here, SFDs are located at the outboard of the supporting hydrodynamic bearings to prevent problems with stability (*Childs, 1993*). These and many other applications have made SFDs valuable elements in high speed turbomachinery.

Figure 1 shows a simplified schematic view of a typical squeeze film damper configuration. The squeeze film damper consists of several components. A journal is press-fitted over the outer race of a ball bearing. To prevent rotation of the journal, a pin or some other restraining mechanism is used. This mechanism allows the restrained journal to whirl (usually at an angular velocity equal to shaft speed.) A very small annular clearance, typically thousandths of an inch, separates the journal from its housing. It is at the clearance where the lubricant is introduced and allowed to flow so as to provide a type of viscous "cushion" for the journal in whirling motion. The whirling motion of the damper journal causes the journal to squeeze the film lubricant against the housing, generating dynamic pressures and hence, fluid film forces opposing the dynamic motion. These are, in brief, the mechanics allowing the damping capability of the SFD.

The force response of SFDs is complex and difficult to predict analytically, although its operation seems quite simple. Theoretical models available are very simplified and do not account for special structural and fluidic characteristics that are essential for the design of SFDs (*San Andres, 1995*). These are only a few of the major reasons why further study of squeeze film damper operation is essential. To aid in the progress of this investigation, experience and controlled

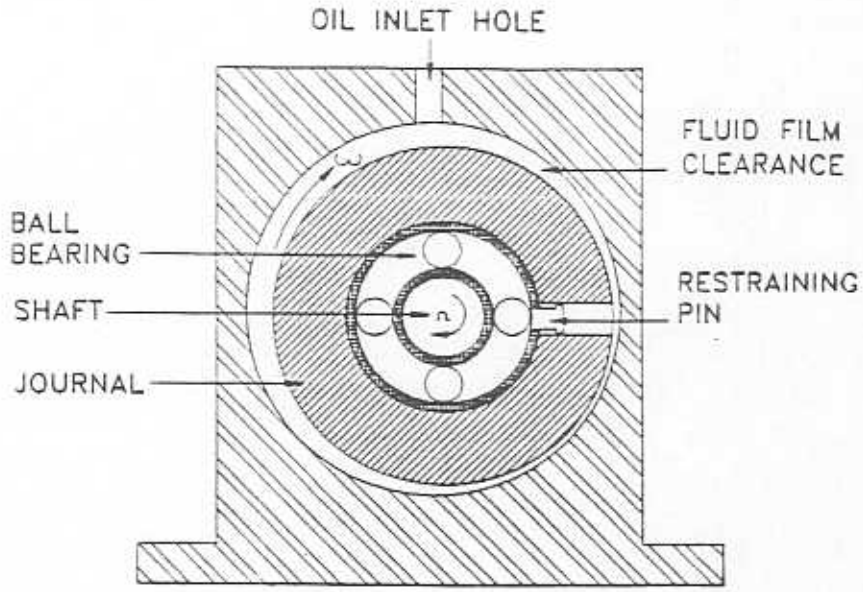

Figure 1. ***Typical Squeeze Film Damper Configuration***

experimentation have identified the following operating conditions as highly influential on the performance of squeeze film dampers:

1. oil feed grooves
2. fluid inertia
3. end seal conditions
4. level of external pressurization and lubricant cavitation

Oil Feed Grooves

The circumferential-feeding groove in a SFD provides a uniform axial flow into the thin film lands. Measurements have shown significant dynamic pressures at the grooves. Hence, SFDs with shallow grooves generate higher fluid film forces which increase their overall damping capacity.

The following experimental investigations on circumferential grooves have shown significant dynamic pressures at the groove and higher damping capacity than predicted by conventional SFD lubrication theory. Roberts et al. (*1986, 1989*) and Ramli et al. (*1987*) obtained experimental force coefficients for a damper with a central groove at different eccentricities. Their results, an order of magnitude greater than their predicted values, laid the suspicion of the groove's responsibility for the discrepancy with lubrication theory. That same year, significant dynamic pressures, about 1/3 of those measured at the film land, were observed at a circumferential feeding groove by San Andres and Vance (*1987a*). Ramli (*1987*) and Rouch et al. (*1990*) noticed that shallow circumferential grooves have a considerable contribution to the force response of SFDs. More recently, Zeidan and Vance (*1990*) obtained dynamic pressure measurements at the groove of about 60% of the ones obtained at the film lands.

Arauz and San Andres (*1993*) demonstrated the significance of a central groove in a SFD force response by testing a grooved damper with sealed and open end conditions. A groove with radial depths of five and ten times the clearance was machined to enhance its effect. Dynamic forces obtained from pressure measurements at the groove were compared to those at the film lands. The results showed significant levels of dynamic pressures generated at the groove. This means that higher tangential and radial forces can be obtained with a grooved SFD. Indeed, due to the large value of the squeeze film Reynolds number, large radial forces were found at the groove. Thus, the circumferential groove induced a large inertia-like effect on the film lands.

Conventional lubrication theory can no longer isolate grooves from the mechanics of the SFD. Grooves interact with the film lands because of the significant dynamic pressure levels that are produced at their locations. Although the groove importance has been revealed, its influential existance has opened the door to other areas of study. For instance, some of the factors thought to have an influence on the damper groove-induced force response are:

1. fluid inertia,
2. enhanced turbulence effects,
3. geometric discontinuities,
4. compressibility of the fluid.

Future investigations of individual or combinations of these factors can be quite valuable.

Fluid Inertia

Fluid inertia has been found to significantly affect the dynamic response of a SFD. Fluid inertia forces appear as an added mass effect in the SFD-rotor system for
the following SFD conditions:

1. large clearance
2. light viscosity oil
3. high frequencies

The squeeze film Reynolds number ($\mathbf{Re}_s = \rho\omega c^2/\mu$) denotes the ratio of inertia forces to viscous forces. For most practical applications, $\mathbf{Re}_s$ varies between 1 and 50 (*San Andres and Vance, 1987 b*).

Tichy (*1984*) and San Andres and Vance (*1987a, b*) demonstrated the importance of fluid inertia effects on the dynamic force response of SFDs. For squeeze film Reynolds numbers larger than 10, experiments showed the influence of fluid inertia. In other words, the radial force was found to be significantly

greater than the damping (tangential) force in the absence of cavitation. Recently, San Andres et al. (*1991 a,b*) tested a large clearance (c /R = .025) SFD at both open and partially sealed conditions. For an orbit radius of 50% of the radial clearance, the dynamic force response was measured at various whirl frequencies. The large clearance SFD tested yielded large squeeze film Reynolds numbers at low whirling frequencies. Thus, significant effects of fluid inertia were produced. Indeed, tests performed with the open end SFD isolated the fluid inertia effect and showed its dependence on the square of the whirl frequency.

Correlation between experimental results and analytical predictions has been anywhere from poor to satisfactory (*San Andres, 1995*), although significant theoretical advancements have been made by Tichy et al. (*1978*), Szeri et al. (*1983*), San Andres and Vance (*1986, 1987a*), and San Andres (*1991c*).

End Seal Conditions

End seals, usually installed to reduce axial flow through a damper, have a large effect on the force coefficients of SFDs (*Vance, 1988*). Figure 2 shows three common end seal configurations for squeeze film dampers. The presence of end seals increases the damping capacity of the SFD. Arauz and San Andres (*1993*) tested a damper for open (no end seal) and partially sealed end conditions. Greater radial and tangential forces were found for the partially sealed case. Unfortunately, accurate knowlege of the end leakage condition is required to predict the damping qualities of these seals.

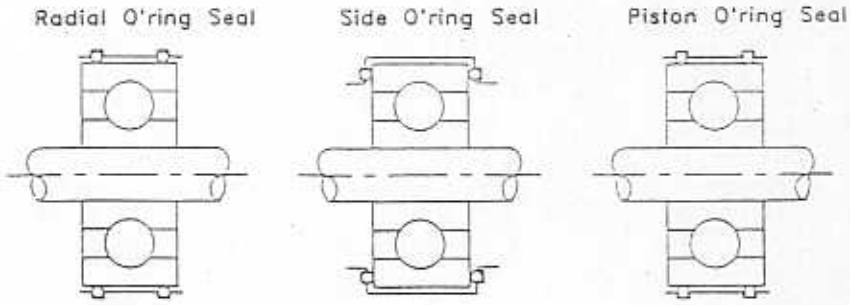

Figure 2. ***Three Typical End Seal Configurations for Squeeze Film Dampers***

External Pressurization and Lubricant Cavitation

External pressurization plays a major role in the operation of a SFD. The ideal operation of a SFD requires a supply pressure level large enough to prevent cavitation of the lubricant. Cavitation of the lubricant occurs at low squeeze film

pressures when either each or a combination of the following conditions exists (*San Andres, 1995*):

1. vaporization,
2. gaseous formation,
3. air entrainment,
4. bubbly mixture formation.

Experimentation and applications have shown that the type of cavitation present and its extent usually depends on the following parameters:

1. whirl frequency,
2. dynamic journal eccentricity,
3. end seals,
4. supply pressure.

Since most of the data base available on cavitation pertains to journal bearings, little is known on the role of cavitation on squeeze film dampers. Hence, in order to enhance the performance of a SFD, it is necessary to understand cavitation. The paragraph that follows summarizes the major advancements that have been made on understanding cavitation in squeeze film dampers.

Because of its importance, dynamic cavitation has inspired many investigations. In his dissertation, White (*1970*) described gaseous cavitation in a SFD. He tested a SFD operating with a circular centered orbit for a range of speeds from 300 to 3,000 rpm. With the aid of a clear polymer sleeve, he was able to observe that the cavitation bubbles did not collapse at high pressure regions. This prompted him to conclude that the bubbles in the high pressure region reduced the level of the squeeze film force. Later, Hibner and Bansal (*1979*) recorded the pressure distribution of a SFD, also operating with a circular centered orbit. The measured pressure distributions did not agree with the analytical pressure distributions obtained from the incompressible lubrication theory. The compressibility of the gaseous cavitation zone was held responsible for the disagreement with the classical lubrication theory. This led the authors to propose a variable-density two-phase fluid model to improve the correlation with the experimental results. Feng and Hahn (*1987*) put this idea into practice and used a two-phase fluid model to compare analytical results to measurements taken from a SFD-rotor test rig. Surprisingly, both the two-phase fluid model and the conventional incompressible lubrication theory were found to agree with the experimental measurements. That same year, a visual study of dynamic cavitation in a SFD operating with circular centered orbits was conducted by Walton et al. (*1987*). Using high speed photography and stroboscopic video, the cavitation zone was recorded. The results-- no two-phase fluid was ever observed! Later, Zeidan and Vance (*1990*) obtained high speed motion pictures of dynamic cavitation in a centered SFD describing circular orbits. Pressure measurements

were made to examine the effect of cavitation on the performance of the damper. The experiments allowed for the identification of three regimes of operation:

1. uncavitated at low speeds,
2. a two-phase fluid formed at high speeds (>1500 rpm),
3. transitional conditions occurred at intermediate speeds.

Because of this finding, a proper transient analysis that models the fluid film forces for each regime was suggested. The presence of vapor cavitation was attributed to end seals, which restricted the entrance of ambient air into the SFD clearance.

EXPERIMENTAL SETUP & PROCEDURE

Description of Test Rig

Figure 3 shows a cross-section of the test rig for an open end, circular-centered orbit squeeze film damper. The damper journal, with an outer diameter of 129.41mm (5.095 in.) and an axial length of 30.73 mm(1.210 in.), is press-fitted over the external race of a ball bearing. The nominal squeeze film radial clearance is 0.381 mm (0.015 in.) In order to compare the experimental results to actual applications, the damper length to diameter and clearance to radius ratios were designed similar to those found in damper configurations for jet engines (L/D = 0.237, C/R = 0.0059).

The journal is mounted off-centered on the shaft by means of an eccentric sleeve which constrains the motion of the journal to a circular orbit about the housing center. The orbit radius at zero rpm is 50% of the radial clearance. Rotation of the journal is inhibited by antirotation "ears" that stem from the journal and are pinned to the housing support.

Lubrication is made possible through two small orifices at the top and bottom sections of the housing. The damper is sealed by installing an O'ring at the left end of the journal. The right end is left open to allow axial flow of the lubricant. Check valves prevent lubricant backflow. The lubricant exits the damper through the top port, since the bottom outlet valve is closed to allow the journal to be fully submerged in the lubricant.

The lubricant used in the tests is SAE 30 engine oil. Prior to the experiment, the specific gravity and viscosity of the oil was measured at ambient pressure and within the operating temperature range of the test rig. Table 1 lists the values of specific gravity and viscosity for different temperatures.

From these measurements, a viscosity-temperature relationship was determined from algebraic formulae based on the standard ASTM D-341. Table 2 shows the numerical parameter needed to correlate viscosity and specific gravity to temperature.

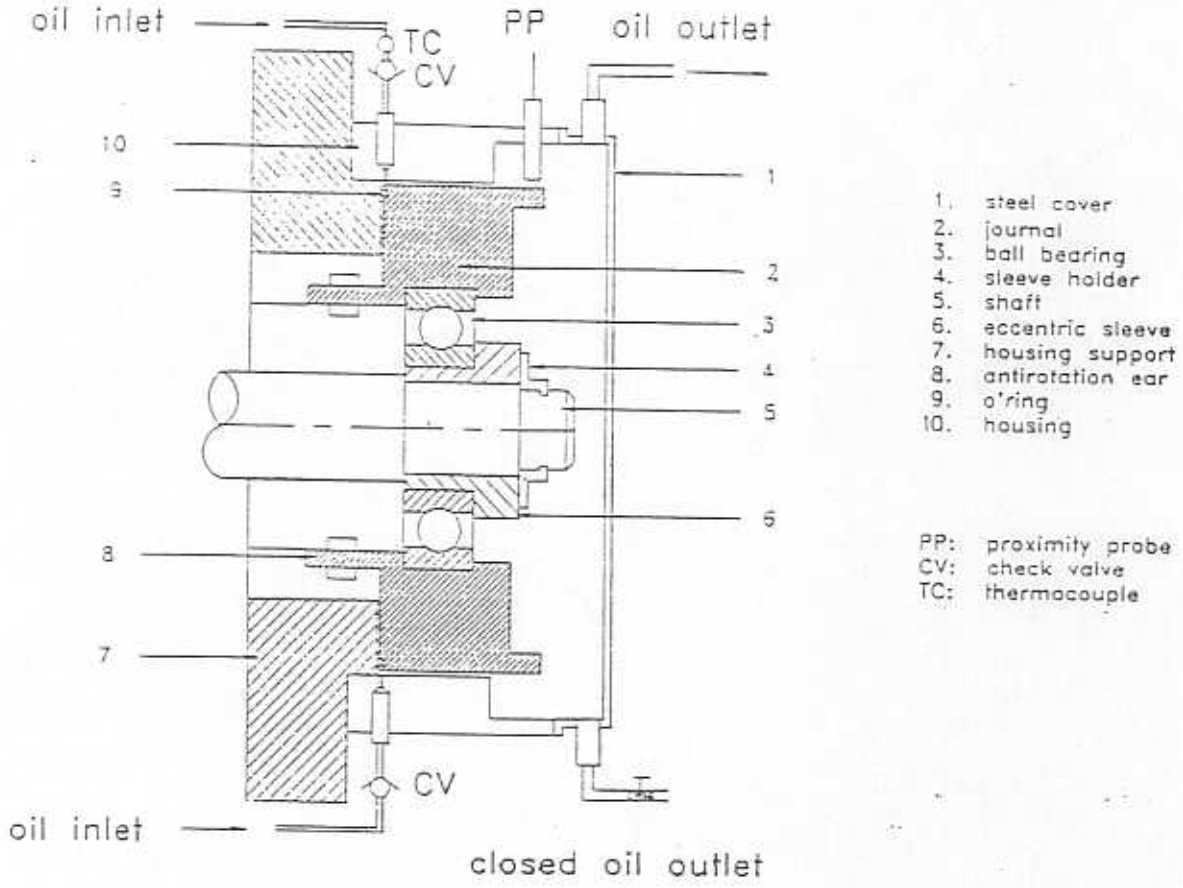

Figure 3. *Front Cross-Section of Squeeze Film Damper Test Rig*

Table 1
Viscosity and Density for SAE 30 oil

Temperature °C	Viscosity Pa-s	Specific Gravity kg/m^3
22	0.230	854.3
28	0.170	851.6
33	0.120	849.4
36	0.110	848.0
39	0.090	846.7
42	0.080	845.3
43	0.075	844.9
46	0.066	843.5
49	0.057	842.2

Table 2
Viscosity & Specific Gravity of SAE 30 Oil
As a Function of Temperature

Specific Gravity (SG, kg/m^3).....$SG = 1000\{ A1 + A2[1.8T(C) + 32] \}$

Viscosity (μ, in centipoise)....$\log[\log(\mu + 0.7)] = B1 + B2\log[1.8T(C) + 491.67]$

where A1 = 9.55395 A2 = -3.36774
B1 = 0.87220 B2 = -0.00025

Figure 4 shows a top cross-sectional view of the test rig. A proximity probe (displacement sensor) is located within the damper housing, directly in front of the journal. Since the damper operates with circular centered orbits, only one proximity probe is needed to measure the displacement of the journal. However, another proximity probe, used to measure vertical journal displacements, allows the monitoring of the journal orbit on an oscilloscope.

The damper bearing whirl frequency is equal to the rotational speed of the shaft and is measured with an optical sensor. The temperature of the lubricant is measured with three thermocouples at the oil inlet valve, film land (z_2), and the oil exit location, respectively. A 10 horsepower, variable speed DC motor drives the shaft through a timing belt and two pulleys with a 2:1 ratio. See Figure 5. (photograph).1

Two piezoelectric pressure transducers are located along the z-axis at positions z_1 (5.59 mm or 0.22 in.) and z_2 (16.70 mm or 0.6575 in.) from the damper's sealed end (Refer to Figure 4). The pressure field is integrated along the circumferential direction to determine the fluid film forces per unit length. Since previous experiments have found identical time variations in the damper circumferential pressure, only one pressure transducer is needed to measure the damper dynamic pressure field. Furthermore, for circular-centered orbits, well known kinematic relationships allow computation of the forces from dynamic pressure measurements at a single fixed location. However, in order to accurately estimate a fluid film force, a second pressure measurement (say, from z_2) allows for the computation of an average. This arithmetic average of the forces at locations z_1 and z_2 approximates axial variations (*San Andres, 1995*).

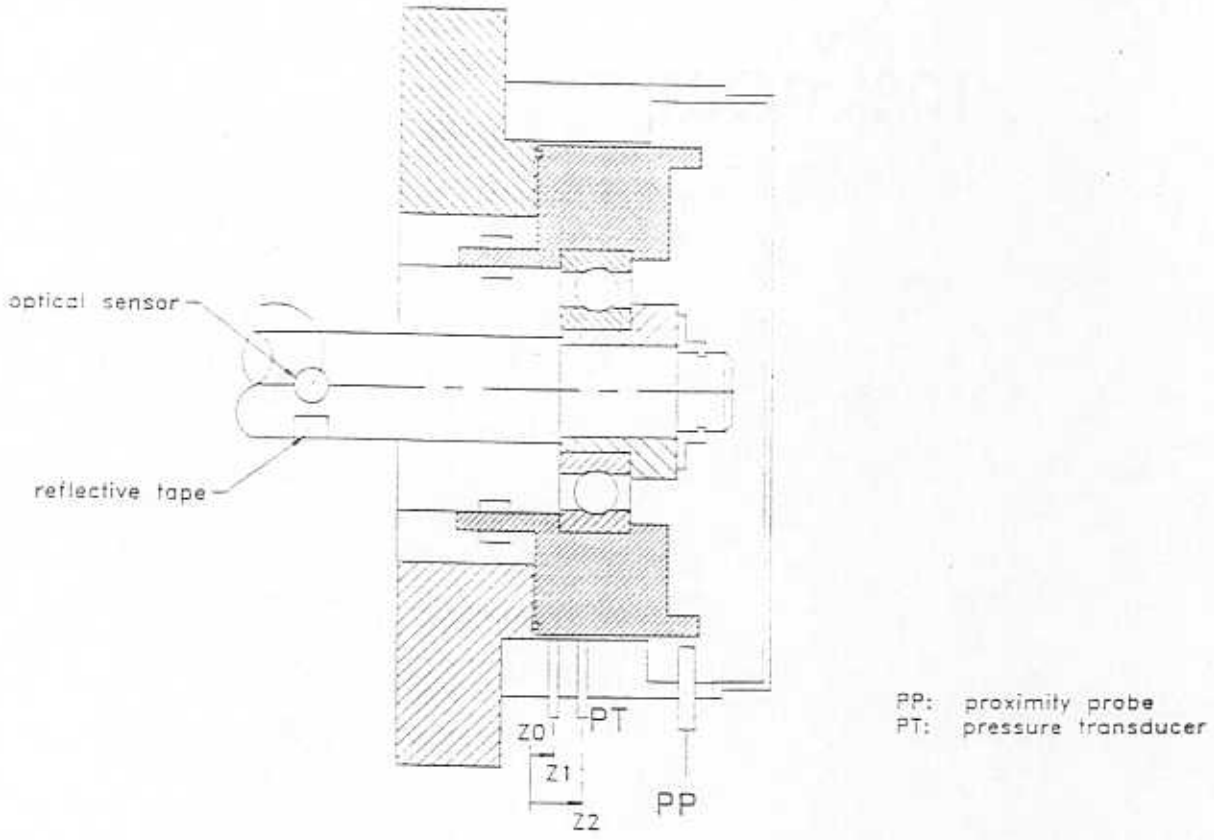

Figure 4. *Top Cross-Section of Squeeze Film Damper Test Rig*

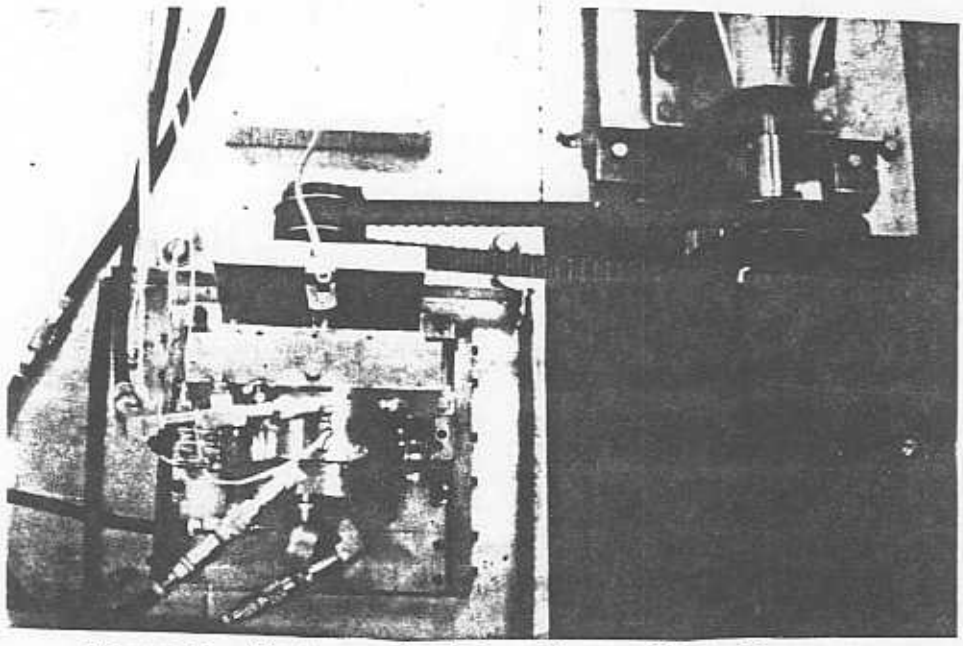

Figure 5. *Photograph of Top View of Test Rig*

Instrumentation and Data Acquisition

Figure 6 shows a schematic of the test rig, its instrumentation and the respective connections.

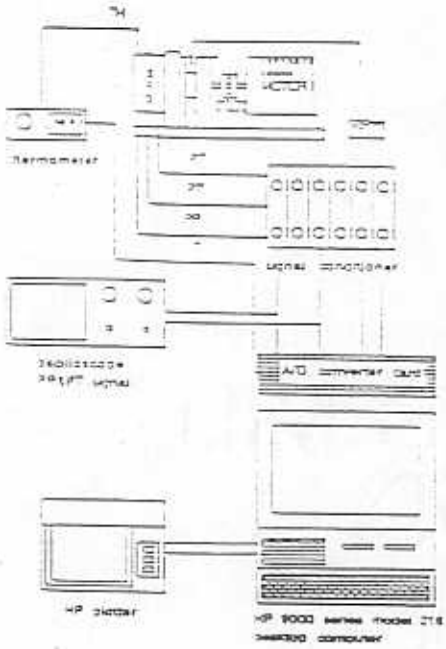

Figure 6. *Diagram of Test Rig & Instrumentation*

For a better view of the instrumentation, see Figure 7.

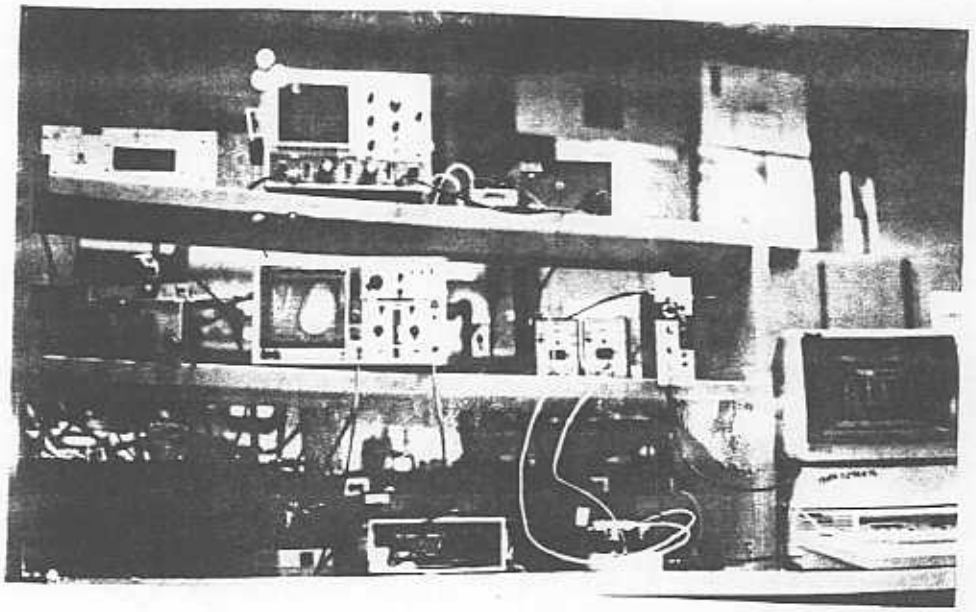

Figure 7. *Photograph of Instrumentation*

Figure 8 shows the main sequence of events that take place within the data acquistion program. The pressure distribution and motion of the journal were measured with 75 data points per cyle of orbital motion. For each test condition (film land temperature), 10 cyles of data were recorded. The forces were calculated from the average of the 10 sets of pressure data. The damping coefficients were calculated by dividing the radial and tangential forces by the jpurnal tangential velocity (eω).

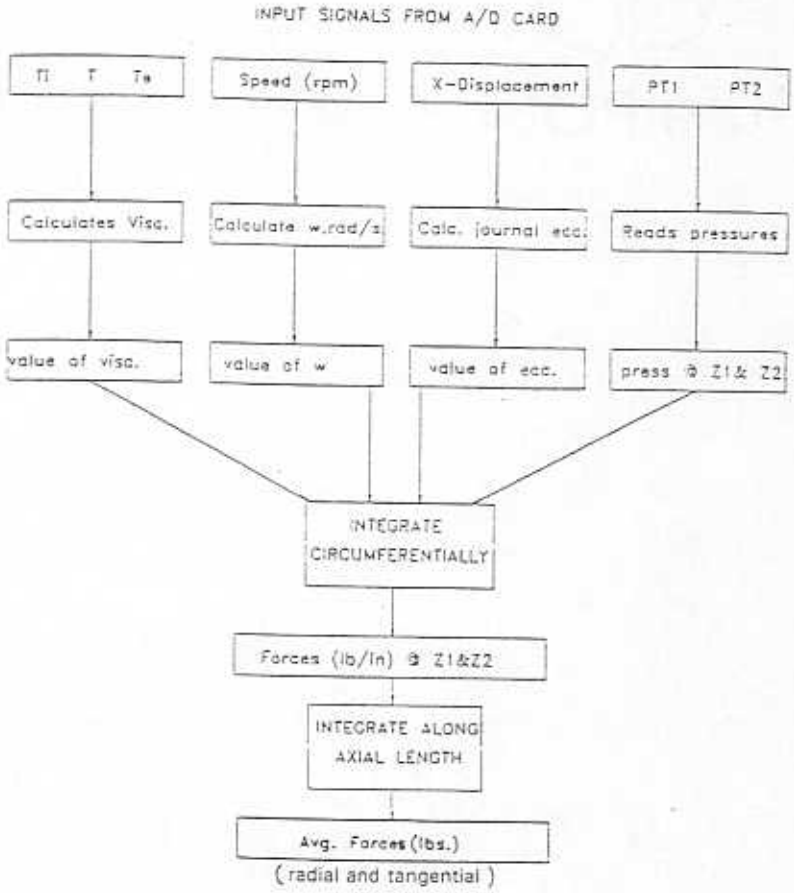

Figure 8. *Flow Chart of Data Acquisition Program*

THEORY

Figure 9 shows a schematic view of a journal describing a circular centered orbit of radius e and at the whirl frequency ω equal to the rotor angular speed. The synchronous motion of the journal encounters an opposing fluid film force that can be broken up into its radial and tangential components as:

$$F_r = -C_{rt} V_t \qquad F_t = -C_{tt} V_t \qquad (1)$$

where C_{rt} and C_{tt} are the cross- and direct damping force coefficients and $V_t = e\omega$ is the tangential speed of the journal. These equations do not account for inertia effects due to the fact that the damper tested was purposely designed with a small squeeze film Reynolds number ($Re_s = \rho\omega c^2/\mu < 1.0$). Analytical determination of the cross- and direct damping coefficients comes from conventional lubrication theory. In essence, a study of the pressure field in the squeeze film damper is necessary (*Vance, 1988*).

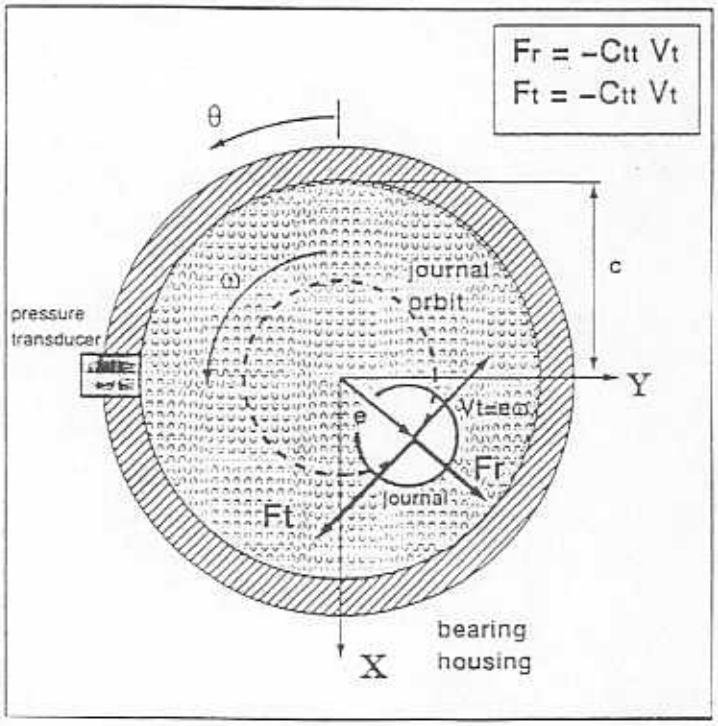

Figure 9. *Schematic of Journal in Circular Centered Motion and Coordinates*

Figure 10 shows a typical pressure distribution around the journal of a squeeze film damper. The schematic view shows that the highest dynamic pressure is produced by the whirling motion of the journal at the region along the tangential velocity vector (squeeze region). The dynamic pressures developed in this region are known as positive pressures. The dynamic pressures at the opposite side of the journal are called negative pressures, since at this location decrease as the journal moves farther away from its housing. From the general form of the Reynolds equation, the pressure distribution for the SFD tested (short length, open ends $L/D \leq 0.25$) is

$$P(\Theta) = P_a - \frac{6\mu\omega\varepsilon\sin\Theta(L^2 - z^2)}{c^2(1 + \varepsilon\cos\Theta)^3} \qquad (2)$$

where μ = viscosity (Pa*sec)
ω = whirl frequency (rad/s)
c = damper radial clearance (m)
P_a = ambient pressure (Pa)
L = length of journal
z = axial coordinate for length of journal
ε = e/c = dimensionless orbit radius
θ = circumferential coordinate

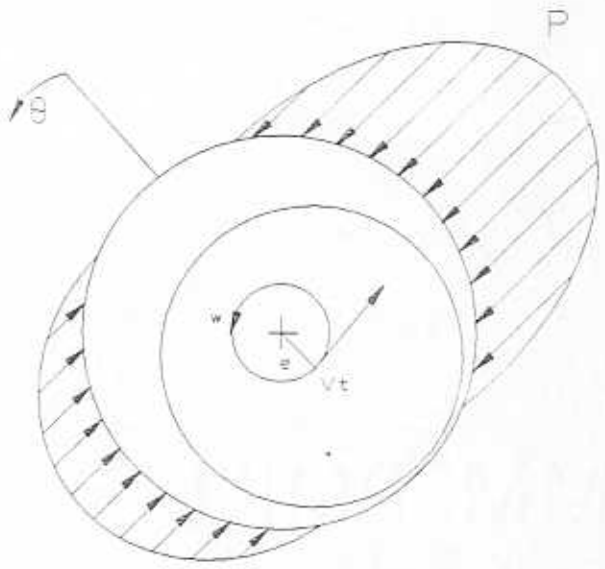

Figure 10. *Schematic Representation of the Pressure Distribution in a Squeeze Film Damper Bearing*

Figure 11 shows a theoretical plot of the dynamic pressure distribution for one cycle of motion. The dynamic film pressure from equation (2) is a parabolic function of the axial coordinate z. Figure 12 shows the parabolic pressure profile assumed for the squeeze film damper tested.

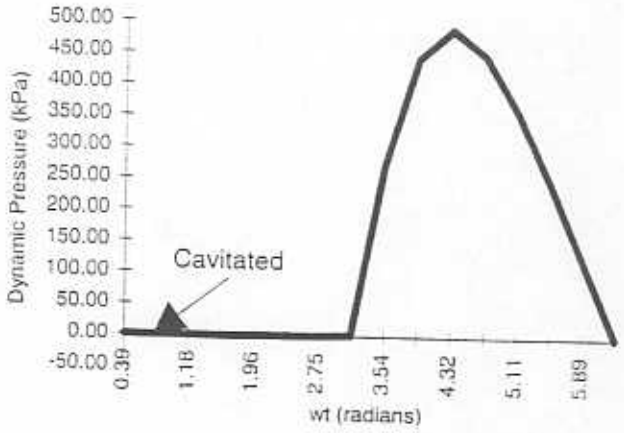

Figure 11. *Theoretical Dynamic Pressure Wave*

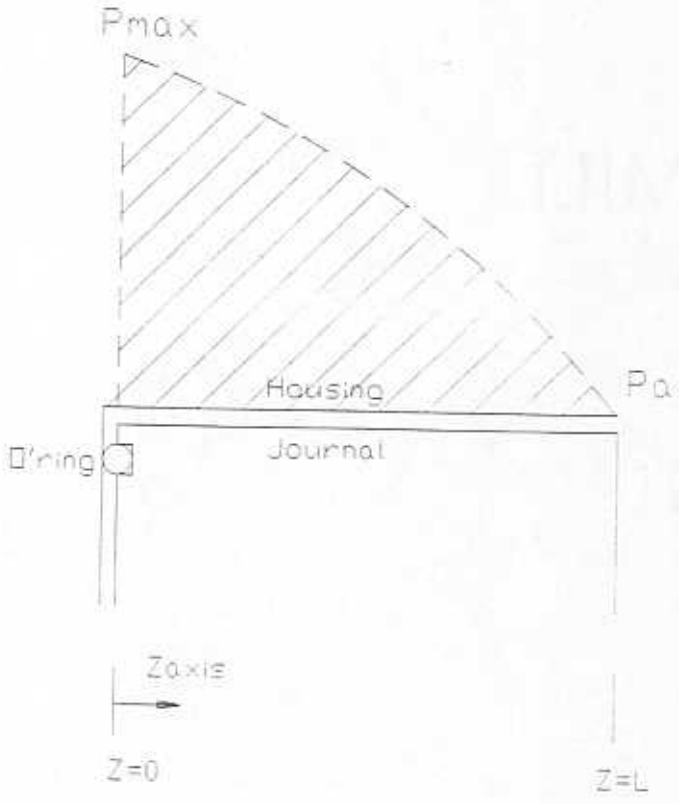

Figure 12. *Assumed Dynamic Axial Pressure Distribution*

Figure 13 shows the pressure profile for a squeeze film damper that is open at both ends and has an effective length equal to 2L.

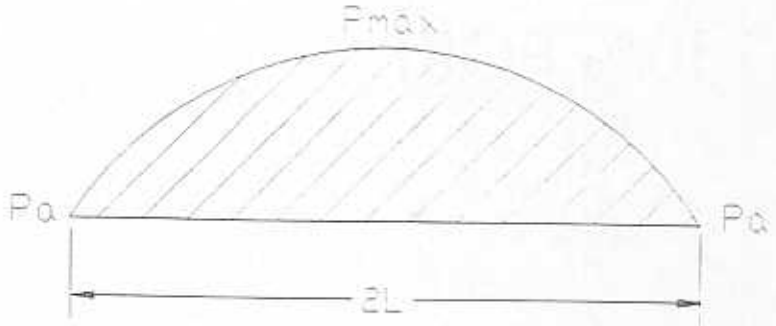

Figure 13. *Dynamic Pressure Profile For a Squeeze Film Damper of Lenght X = 2L and Open at Both Ends*

By assuming the pressure profile just presented, the incompressible π-film lubrication theory yields the following radial and tangential forces:

$$F_r = -\frac{\mu D X^3 \omega \varepsilon^2}{c^2(1-\varepsilon^2)^2} \qquad F_t = -\frac{\pi \mu D X^3 \omega \varepsilon}{4c^2(1-\varepsilon^2)^{3/2}} \qquad (3)$$

For the damper studied, sealed at one end and with length $L = X/2$, its forces will be ½ of those just presented, i.e.

$$F_r = \frac{-4\mu D L^3 \omega \varepsilon^2}{c^2(1-\varepsilon^2)^2} \qquad F_t = -\frac{\pi \mu D L^3 \omega \varepsilon}{c^2(1-\varepsilon^2)^{3/2}} \qquad (4)$$

From these equations, the cross and direct damping coefficients are given as:

$$C_{rt} = \frac{4\mu D L^3 \varepsilon}{c^3(1-\varepsilon^2)^2} \qquad C_{tt} = \frac{\pi \mu D L^3}{c^3(1-\varepsilon^2)^{3/2}} \qquad (5)$$

For the case of no cavitation, the 2π-film model presents the direct damping coefficient as twice the value obtained from the π-film theory. The full film model does not present a cross-coupled damping, i.e. $C_{rt} = 0$ (*Vance, 1988, San Andres, 1995*).

EXPERIMENTAL RESULTS AND DISCUSSION

To determine the effect of viscosity variation on SFD response, three tests were conducted at constant rotor speed and from room temperature until the temperature of the lubricant at the film land reached 46 °C (115 °F). The tests were performed at shaft speeds of 2,000, 3,000 & 4,000 rpm with a supply pressure of approximately 0.069 MPa (10 psi). To determine the effect of oil supply pressure, two other sets of tests at a constant speed of 3,000 rpm were conducted at 0.137 and 0.206 MPa (20 and 30 psi, respectively) for the same temperature range.

Tests for Increasing Whirl Frequencies

The effect of viscosity on the journal orbit radius for a range of whirl frequencies and at 69 kPa supply pressure is presented in Figure 14. Note how the orbit radius decreases linearly with increases in the oil viscosity. The orbit radius is largest at the lowest frequency, 33 Hz. For higher frequencies, 50 and 67 Hz, the journal orbit radius is smaller. The measured orbit radius decreases from its static value of 0.5 at zero rpm due to the large SFD forces that are produced at increasing whirl frequencies. These forces try to center the rotor by deflecting the shaft.

Figure 15a and b show the effect of viscosity on the peak to peak dynamic pressures at locations z_1 and z_2. These tests were taken over a range of operating frequencies with a supply pressure of 69 kPa. Notice how the peak-peak pressures are largest at location z_1, nearest to the sealed end. Error bars are randomly provided to show the standard deviation of over 10 cycles of pressure data. Both figures show increasing peak to peak pressures for increasing values of oil viscosity. The lowest peak to peak pressures occur at 33 Hz. This is reasonable, since at lower operating frequencies, the journal is predicted to squeeze the lubricant more softly than at higher frequencies. The higher the frequency, the faster and harder the journal will squeeze the oil and the higher the pressures that will be produced (greater force generated). The amount of scatter in the peak to peak pressures at 50 and 67 Hz shows the closeness between these data sets. This also explains the closeness in the orbit radius values at these two higher frequencies. Since the orbit radius is constantly changing, the peak-peak pressures were divided by the orbit radius (measurements are shown in Figures 16a and b). Without the orbit radius effect, the dynamic peak-peak pressures show a more linear relationship with viscosity. However, the closeness in the data at 50 and 67 Hz still persists.

Figure 17 shows typical gaseous and vapor cavitation pressure plots for one cylce of journal motion, as obtained from the experimental work of Zeidan and

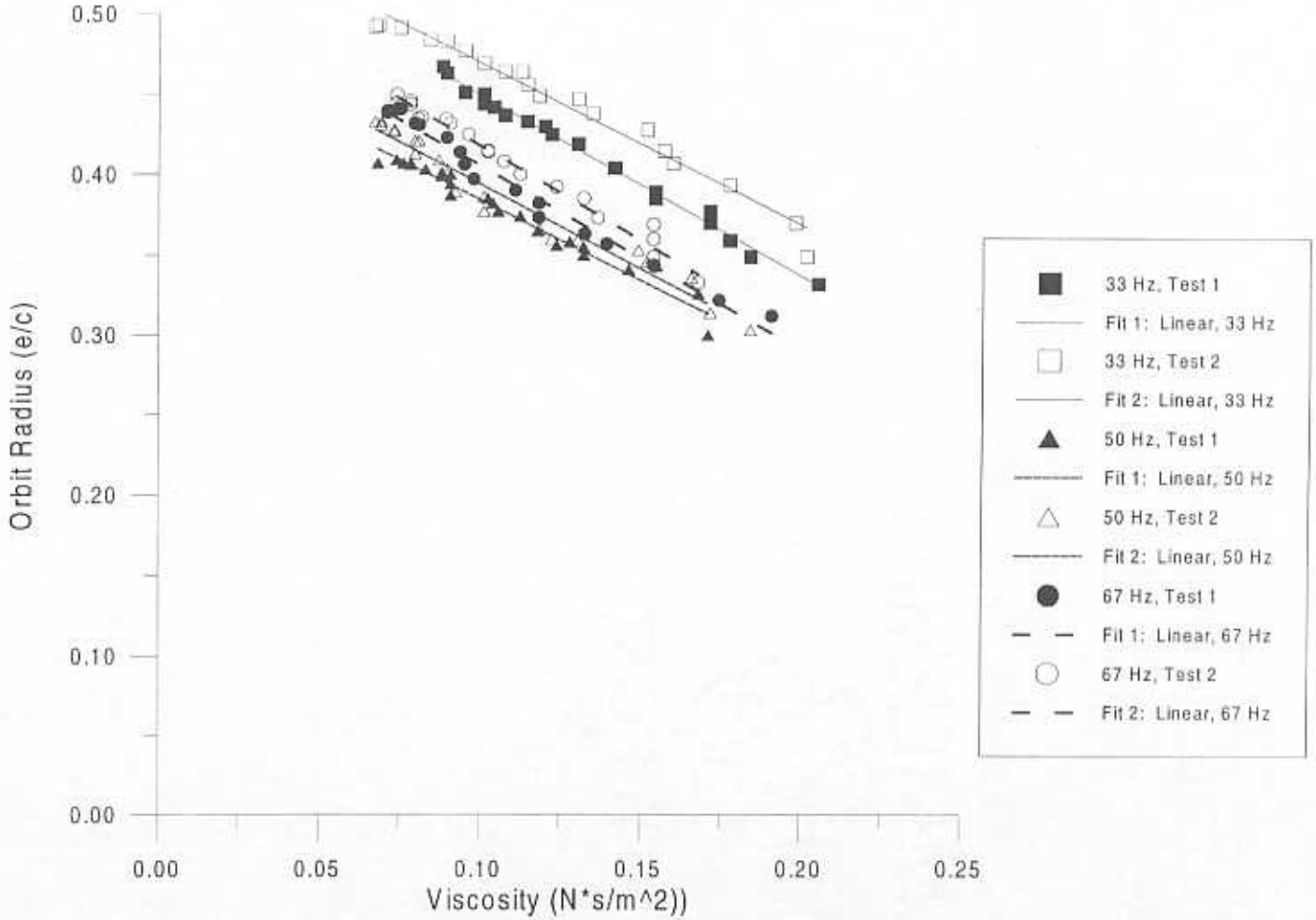

Figure 14.
Effect of Viscosity on Orbit Radius
at Different Whirl Frequencies
(SAE 30 Oil, PS @ 69 kPa)

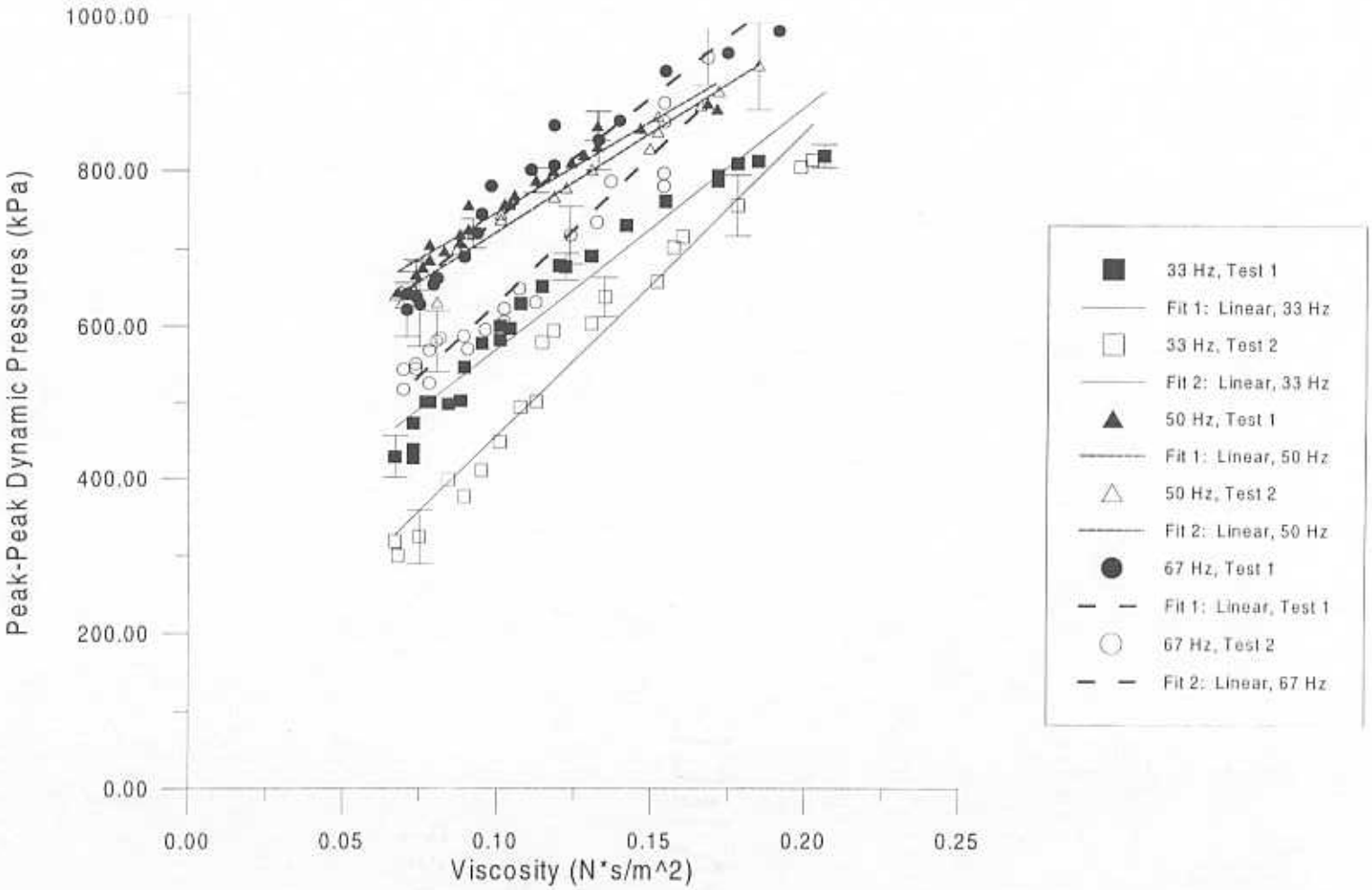

Figure 15a.
Effect of Viscosity on Peak-Peak Dynamic Pressures
at Different Frequencies
(SAE 30 Oil @ 69 kPa , Z1)

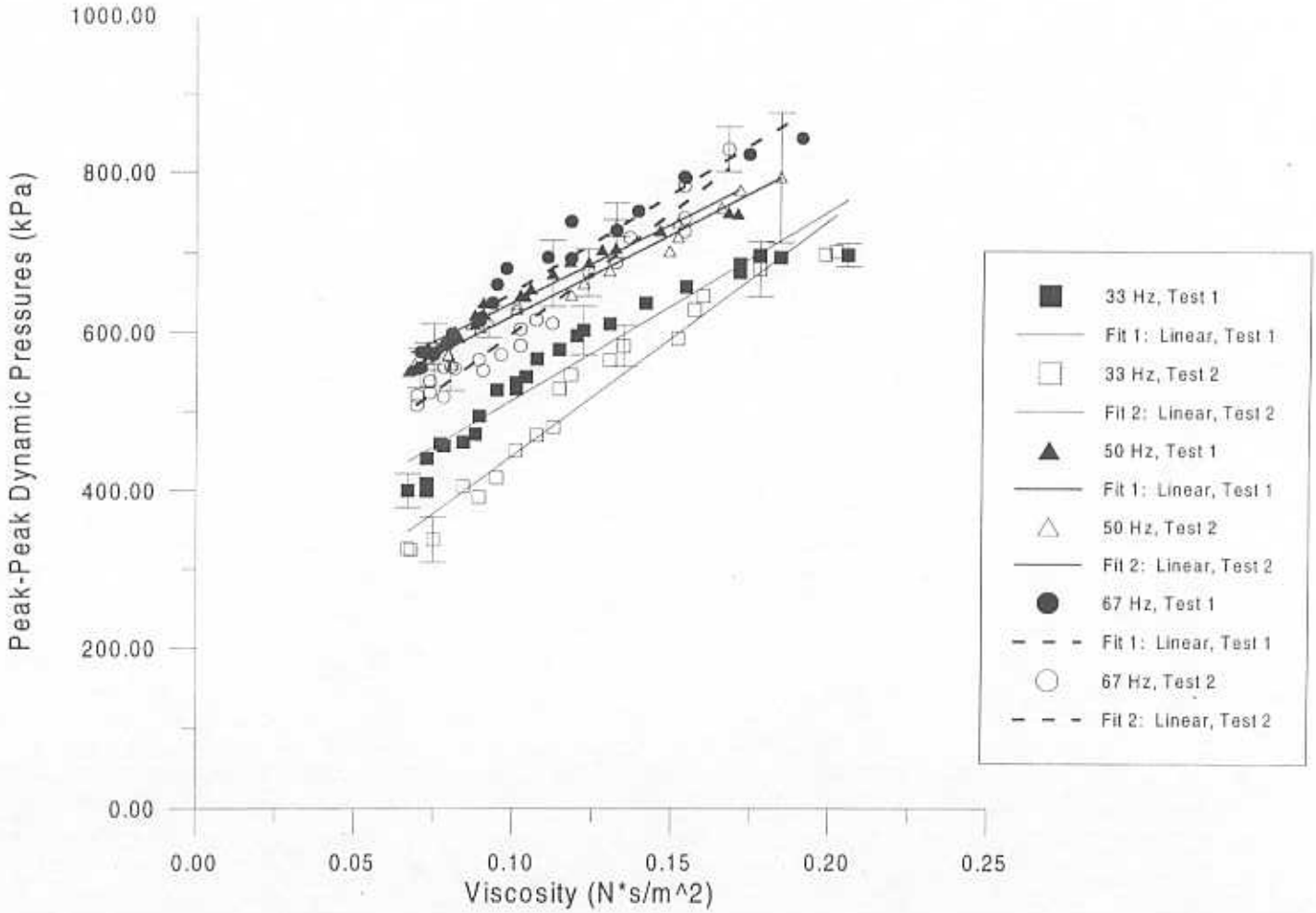

Figure 15b.
Effect of Viscosity on Peak-Peak Dynamic Pressures
at Different Frequencies
(SAE 30 Oil @ 69 kPa , Z2)

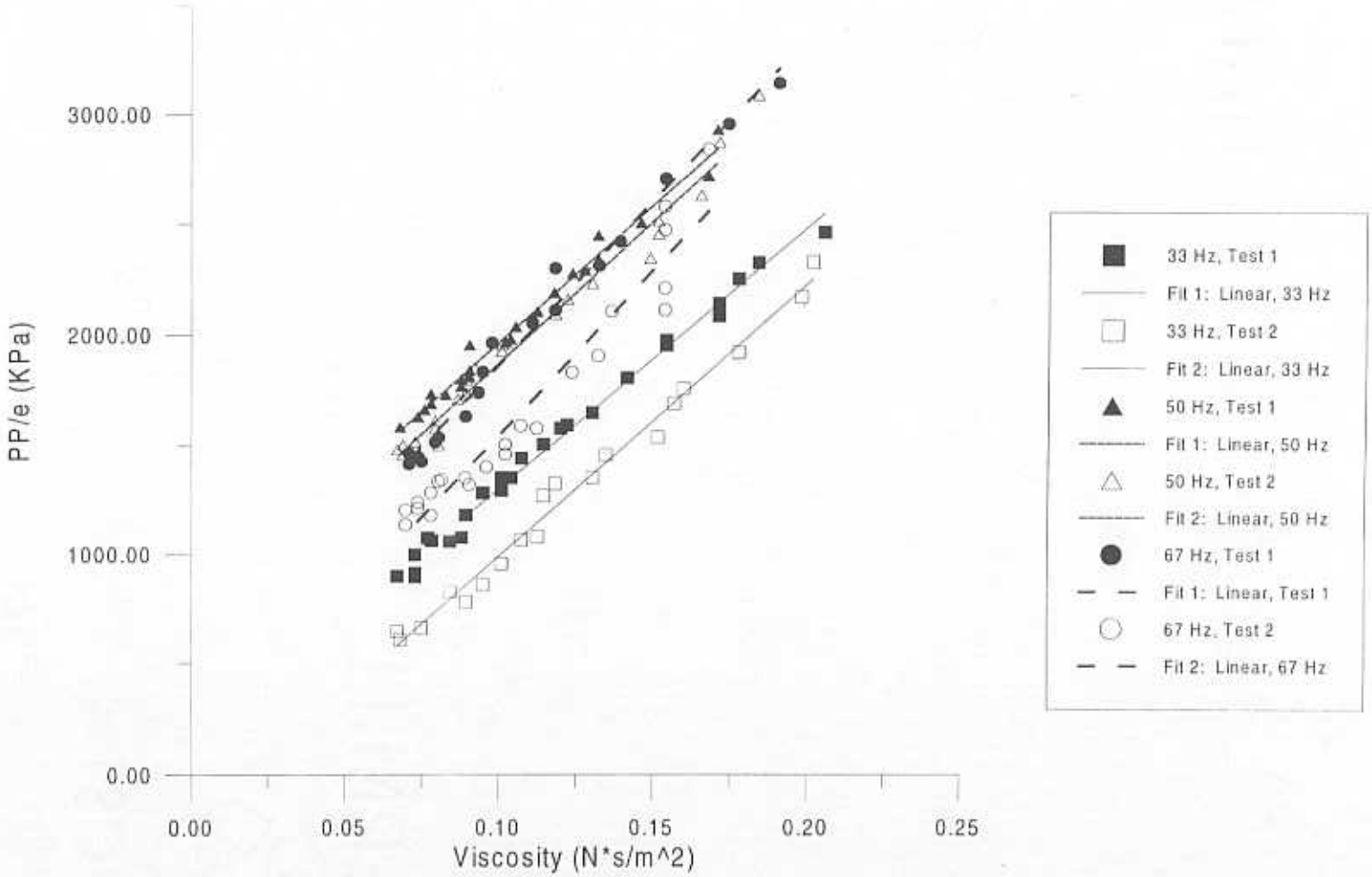

Figure 16a.
Effect of Viscosity on Peak-Peak Dynamic Pressures/Orbit Radius at Different Frequencies (SAE 30 Oil @ 69 kPa , Z1)

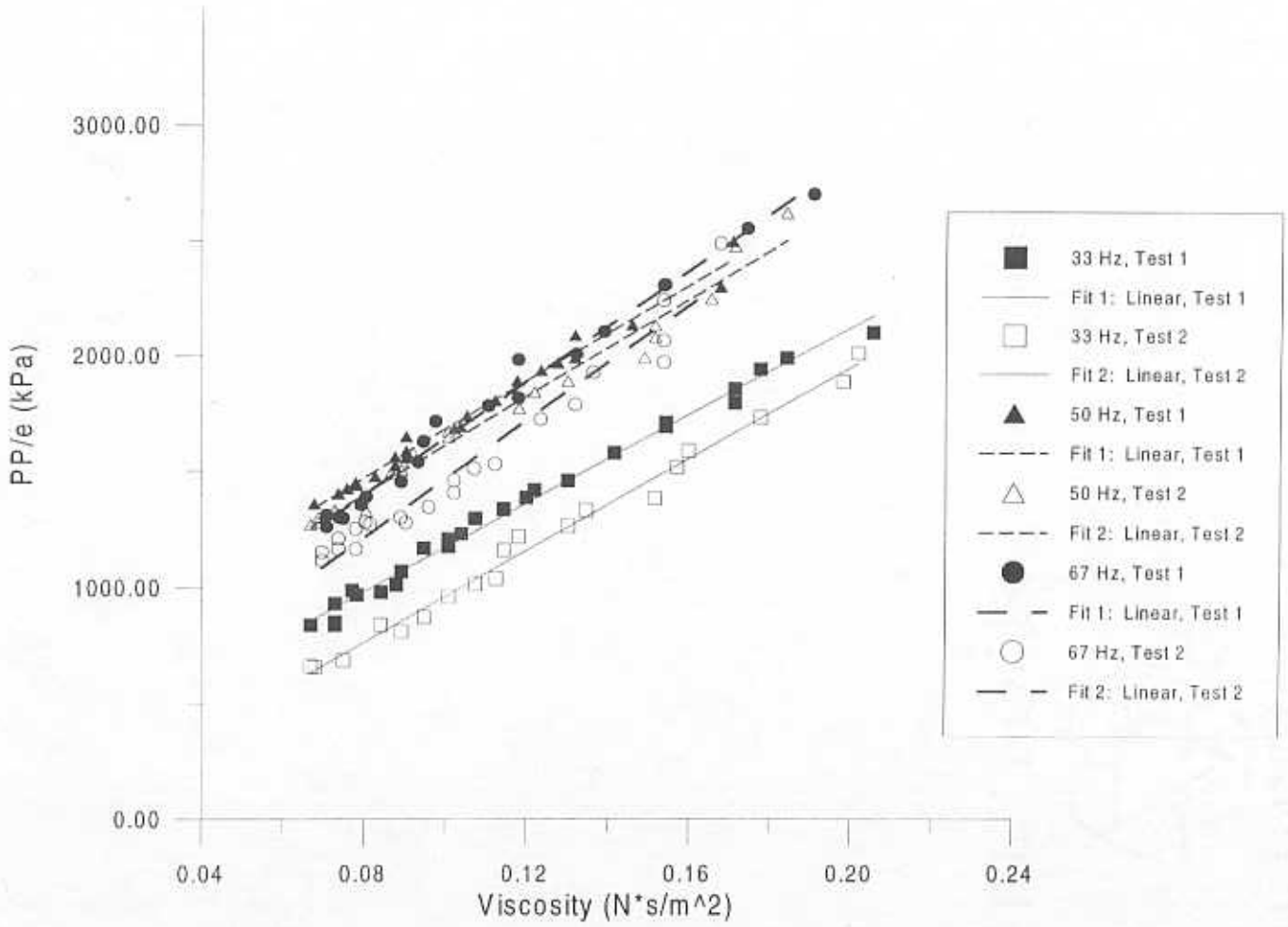

Figure 16b.
Effect of Viscosity on Peak-Peak Dynamic Pressures/Orbit Radius at Different Frequencies (SAE 30 Oil @ 69 kPa, Z2)

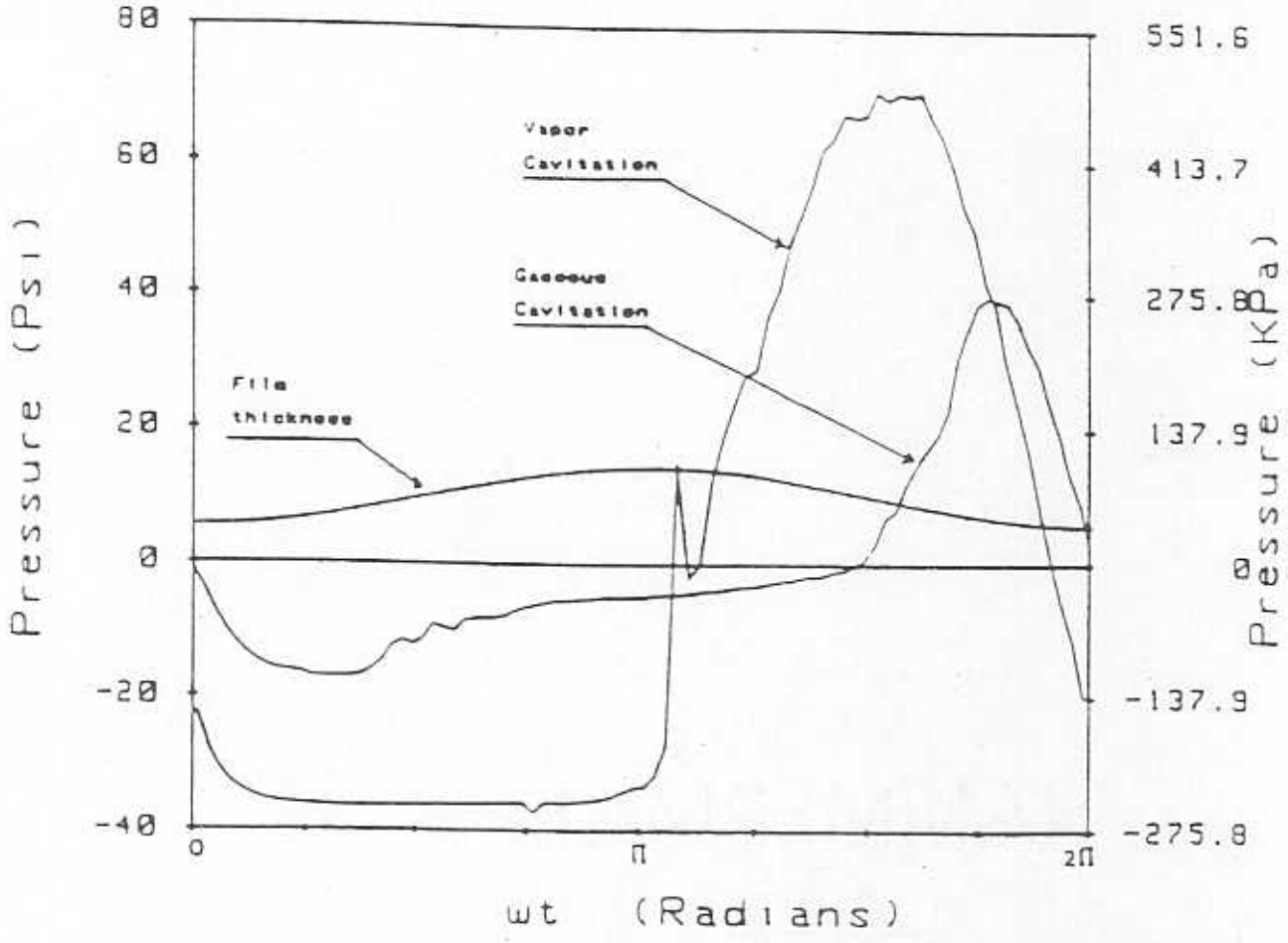

Figure 17. *Pressure Distributions with the Presence of Gaseous and Vapor Cavitation (Taken from Zeidan and Vance, 1990)*

Vance (*1990*) for a squeeze film damper with the following configuration: D = 166 mm, L = 25.4mm, c = 0.635 mm and $\varepsilon = 0.45$. These pressure plots were compared to the experimental results to determine the type of cavitation present in the damper tested.

Figures 18 and 19 present dynamic pressures at axial locations z_1 and z_2 obtained at high and low oil viscosities for increasing values of whirl frequency. The figures also include the variation of the film thickness from the location of the proximity probe (See Figure 4). Measurements were selected at similar orbit radii and squeeze film viscosities for easy comparison. All tests were conducted with a lubricant supply pressure of 69 kPa. As with the peak-peak pressures, the largest dynamic pressure measurements were obtained at location z_1 since it is nearest to the sealed end. Each graph (Figures 18 and 19) shows a plot of the dynamic pressure distribution that is produced during one full cycle of journal motion. For journal motions $\omega xt \leq \pi$ of an entire cycle, the pressure decreases to zero absolute pressure. This occurs when the journal is at its maximum distance away from the pressure transducer. As the journal begins to approach the location of the pressure transducer ($\omega xt > \pi$), the pressure levels off to ambient pressure. Then, the dynamic pressure increases to a maximum value when the journal presses against the housing or squeezes the oil to a minimum value of the clearance. As the journal moves away from the pressure transducer, the cycle is repeated.

From figures 18 we conclude that dynamic pressures increase with increasing values of operating frequency. Note that the extent of the cavitation zone increases with increases in operating frequency. The figure also shows that the maximum dynamic pressures only extend over 1/4 of the journal orbital motion. According to Zeidan and Vance (*1990*), the flat portions of the pressure waves can be interpreted as vapor cavitation, while the jagged portions represent the presence of air or gaseous cavitation. The present results show a combination of both.

Figures 19 depict dynamic pressures measured at low squeeze film viscosities for a range of frequencies. These dynamic pressure measurements are smaller (in magnitude) than the ones in Figures 18, since the rise in temperature of the lubricant has decreased its viscosity. Nevertheless, increases in operating frequencies are also accompanied by respective increases in dynamic pressures and the extent of the cavitation zone. The extent of the vapor cavitation zone increases with increases in whirl frequency. The dynamic pressure distributions for the test frequency of 210 rad/s show maximum pressures extending over 1/8 of the journal's cycle of motion, while at the greater frequencies this occurs over 1/4 of an entire cycle of motion. Comparison of these dynamic pressure distributions to the ones obtained by Zeidan and Vance (*1990*) may indicate the presence of both gaseous and vapor cavitation. However, the configuration of the test rig does not allow for any air entrainment. This means that only vapor

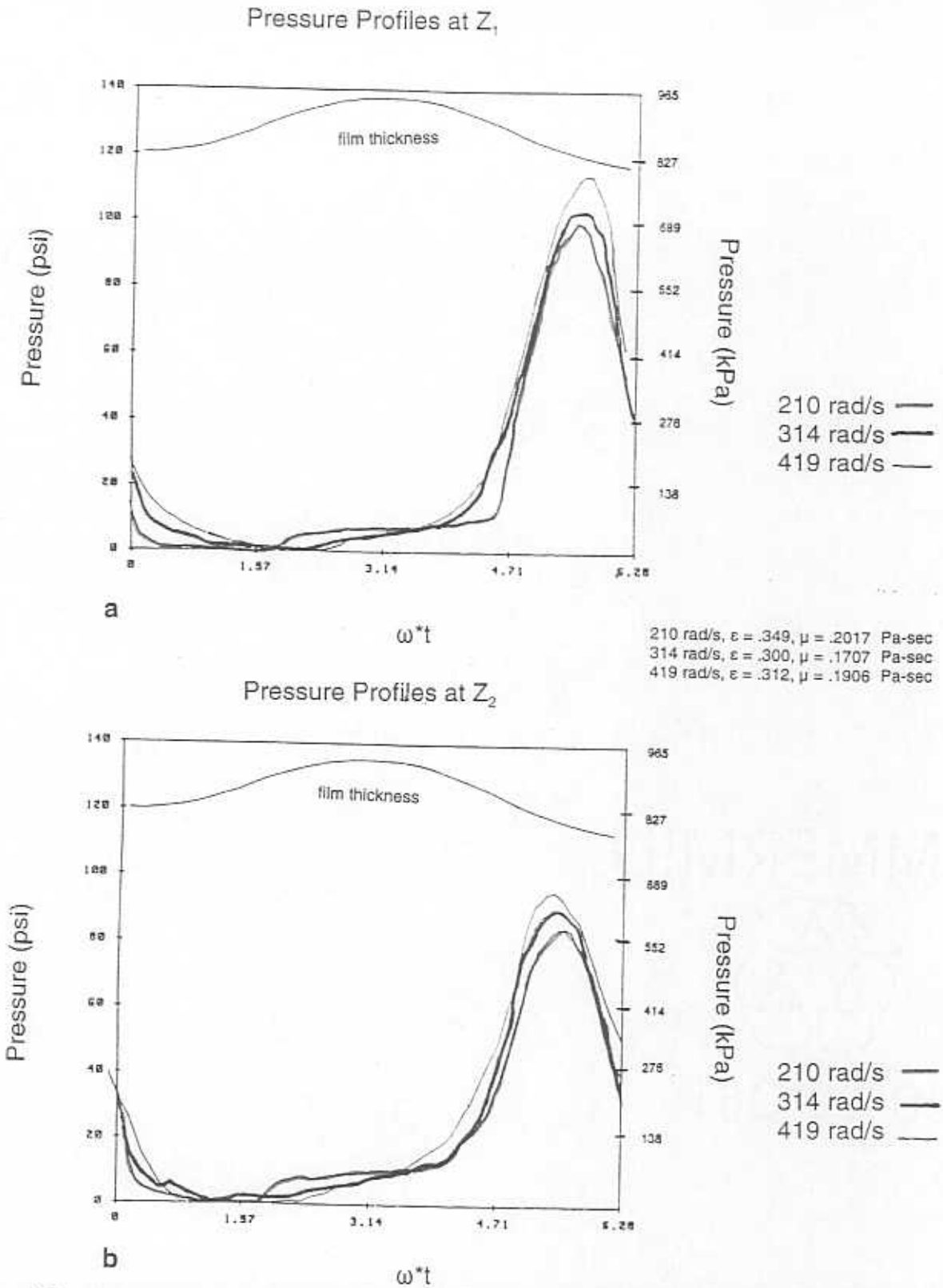

Figure 18 ***Absolute Pressure vs. Time for Increasing Values of Whirl Frequency With 69 kPa Supply Pressure and at High Values of Viscosity***

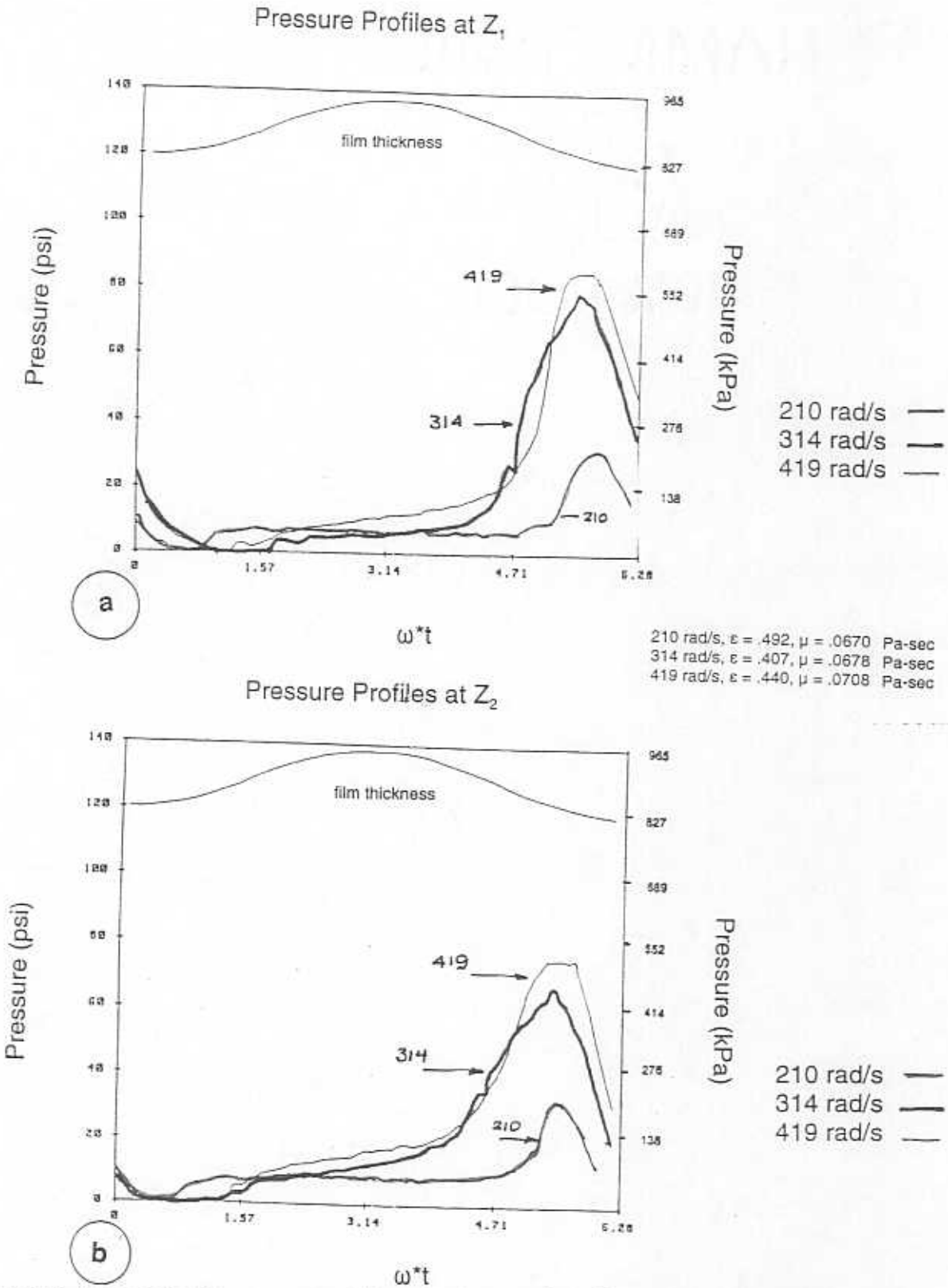

Figure 19 *Absolute Pressure vs. Time for Increasing Values of Whirl Frequency With 69 kPa Supply Pressure and at Low Values of Viscosity*

cavitation is expected to occur. The only way air could infiltrate the film land would be if it were already in the oil. This possibility does exist since the oil had been used prior to these experiments.

A peculiar observation was made at 33 Hz for the low viscosity tests. With the aid of an oscilloscope, alternating expansions and constractions of the peak-peak magnitude of the dynamic pressure waves were observed. Figure 19c consists of ten cycles of raw pressure data at 114°F. Note the variation in the peak to peak pressures.

The relation between the radial force and oil viscosity for increasing whirl frequencies is shown in Figure 20. The graph shows a linear relationship between the radial force and viscosity. The smallest radial forces are produced at 33 Hz, while the largest radial forces develop at the higher frequencies. Recall that increasing the whirl frequency reduces the orbit radius (from Figure 14). Thus, if the radial force is trying to center the rotor by deflecting the shaft of known stiffness, the radial force must be greater at higher frequencies to reduce the orbit radius. Again, the data at 50 and 67 Hz overlaps due to the closeness of the peak to peak pressures at these two data sets.

Figure 21 presents the effect of viscosity on the tangential force for tests at 33, 50 and 67 Hz. The tangential force increases linearly with increasing viscosity. The smallest tangential forces were produced at 33 Hz. These were followed by the data at 67 Hz, making the tangential forces at 50 Hz the highest. These results (the tangential forces at 67 Hz in between the two other frequencies) are no surprise. Figure 14 shows smaller orbit radii for the tests at 50 Hz, and Figures 15 and 16 show the peak to peak pressures at 67 Hz between the data at 33 and 50 Hz.

The effect of viscosity on the direct and cross-coupled damping coefficients can be observed in Figures 22 and 23, respectively. The direct damping coefficient (C_{rr}) increases with increases in lubricant viscosity. For increases in frequencies, the direct damping coefficient seems to decrease. However, the data collected at 33 Hz falls in between the direct damping coefficients at 50 and 67 Hz. This reinforces the fact that the direct damping coefficient is independent of frequency (See equation (5)). The data at 50 Hz tends to agree more with the experimental results of San Andres (1995) than the rest. The cross-coupled damping coefficient (C_{rt}) also increases for increases in lubricant viscosity. The cross-coupled damping coefficients at 50 Hz show a well defined linear relationship with viscosity. Like the direct damping coefficients,the cross-coupled damping coefficients decrease slightly with increases in frequency. The values of C_{rt} that were obtained at 50 Hz also show good correlation with the experimental results of San Andres (1995).

Figures 24 and 25 compare the experimental radial and tangential forces to

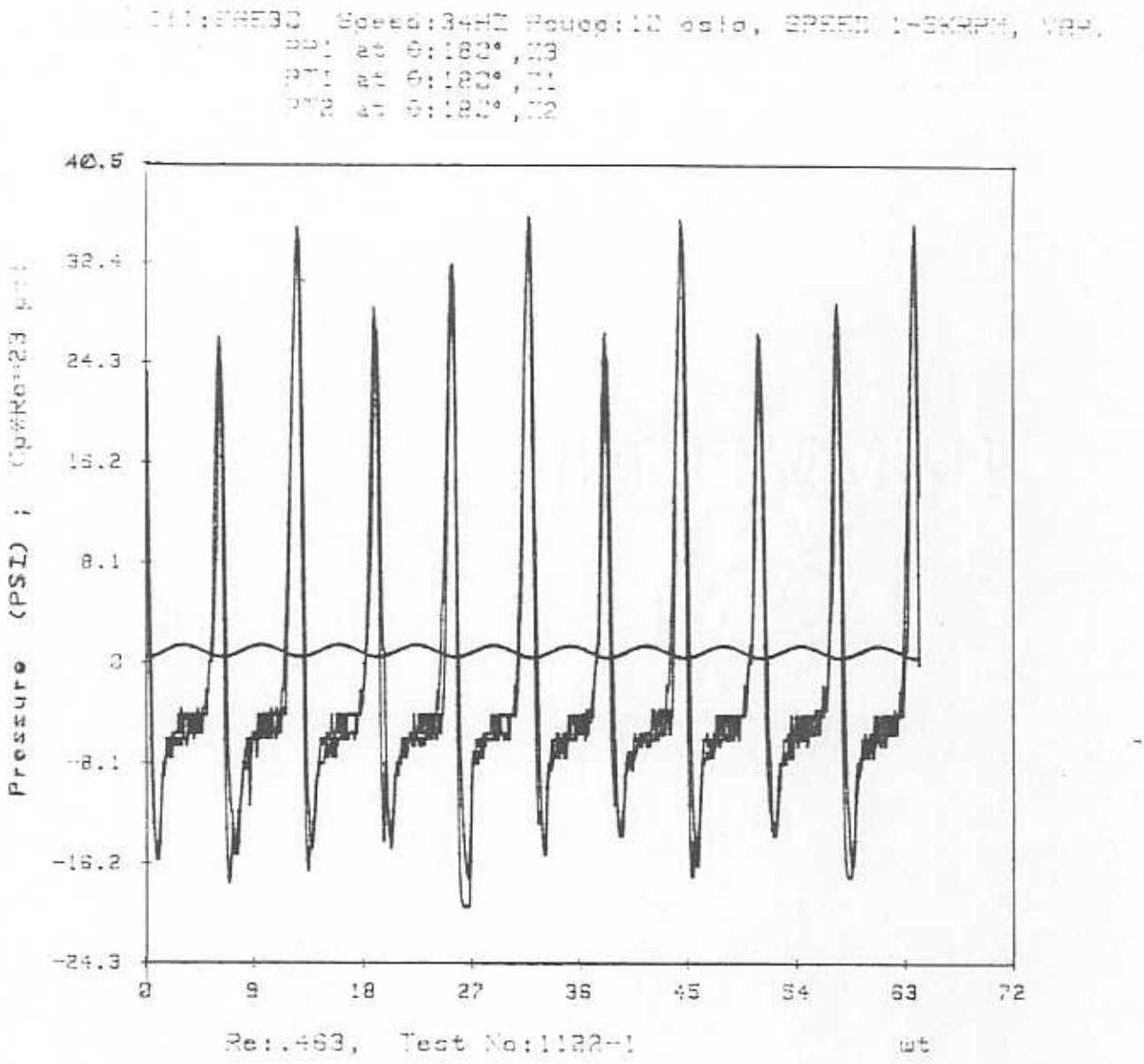

SFD-TRC small c=15 mils, e=7.5 mils, SAE 30 e/c:.492, 34HZ, 110°F

Figure 19c. ***Raw Data: Pressure Distributions at 210 rad/s, 114°F, @ 69 kPa Supply Pressure***

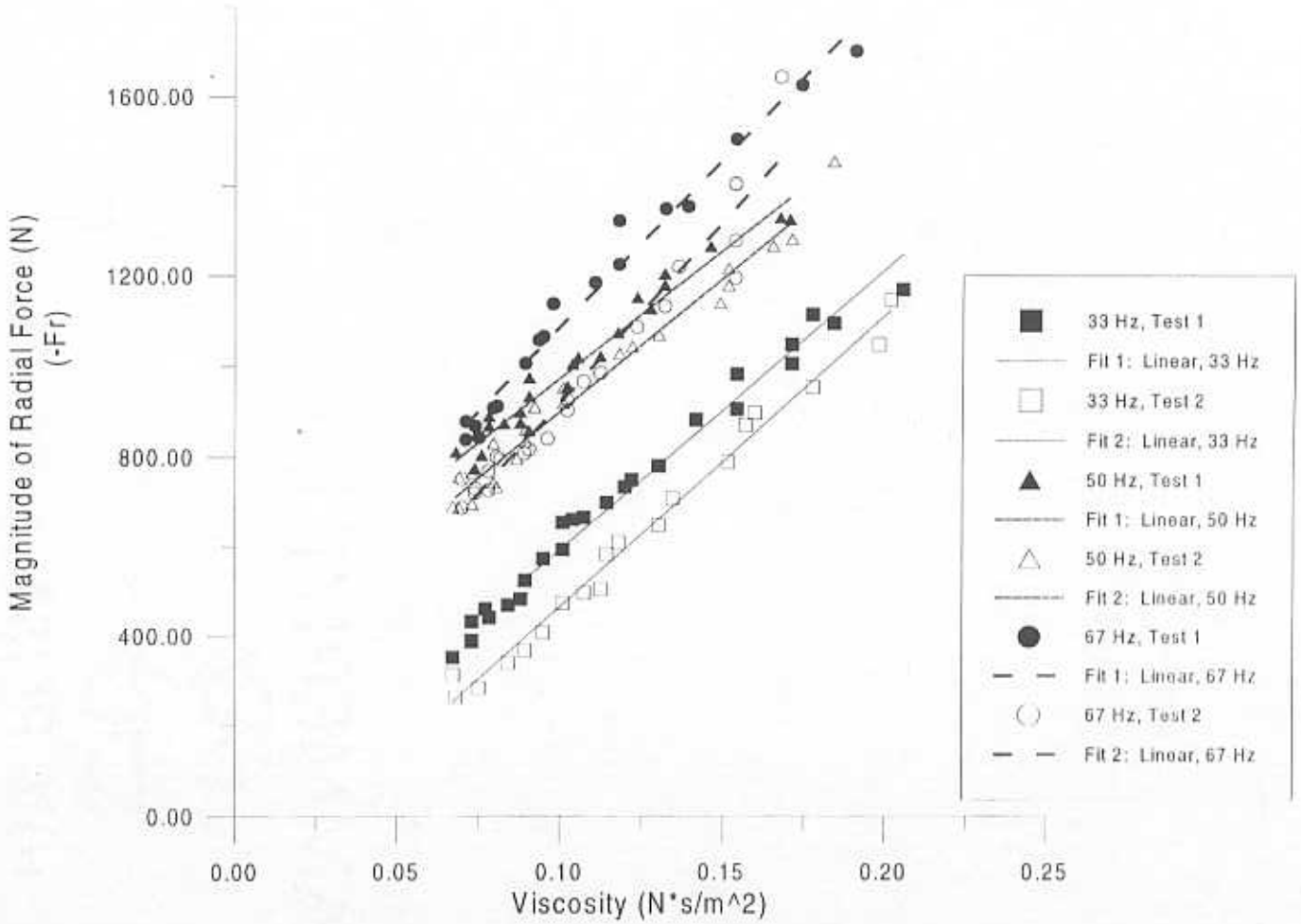

Figure 20.
Effect of Viscosity on Radial Force
at Different Frequencies
(SAE 30 Oil @ 69 kPa)

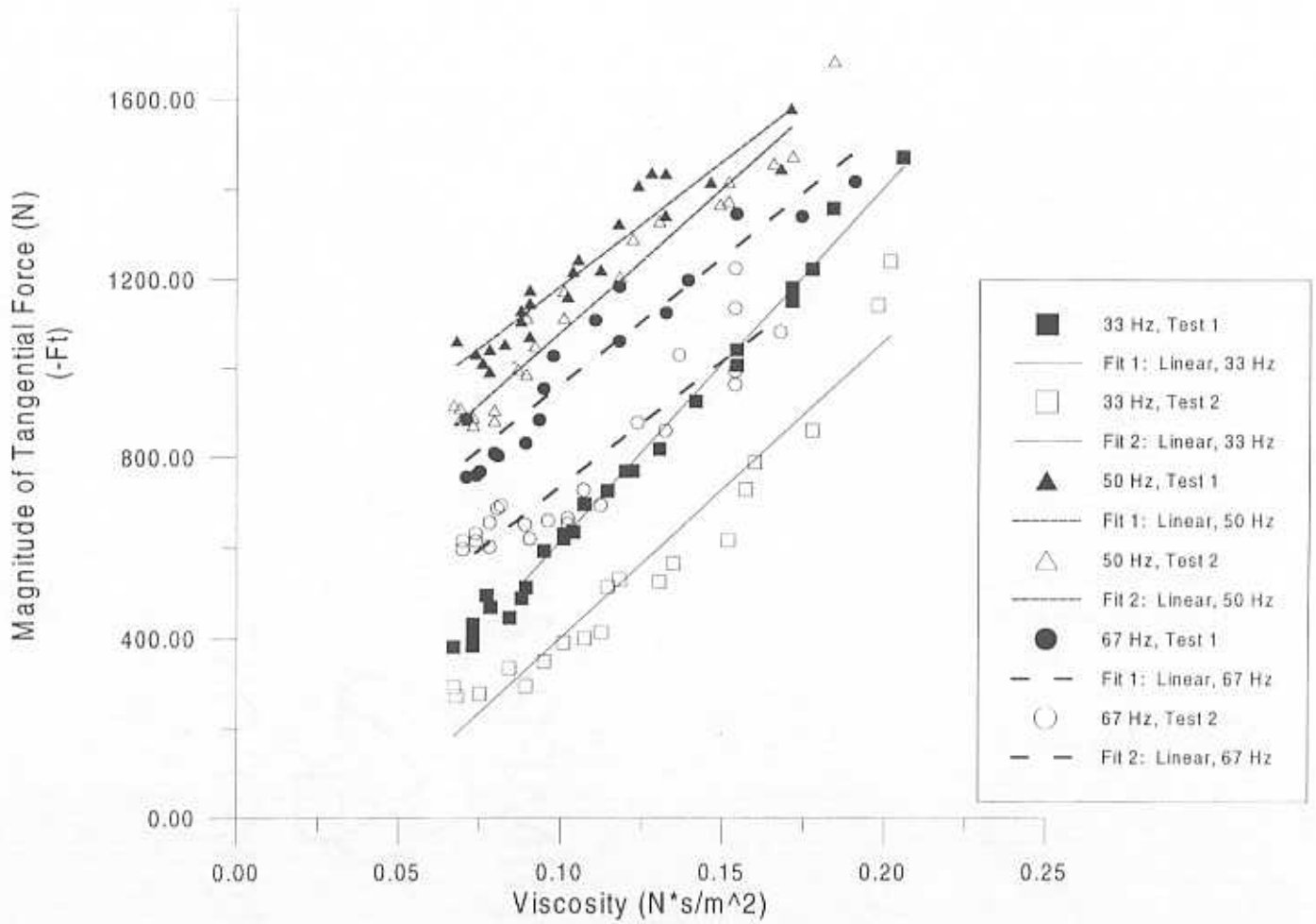

Figure 21.
Effect of Viscosity on Tangential Force
at Different Frequencies
(SAE 30 Oil @ 69 kPa)

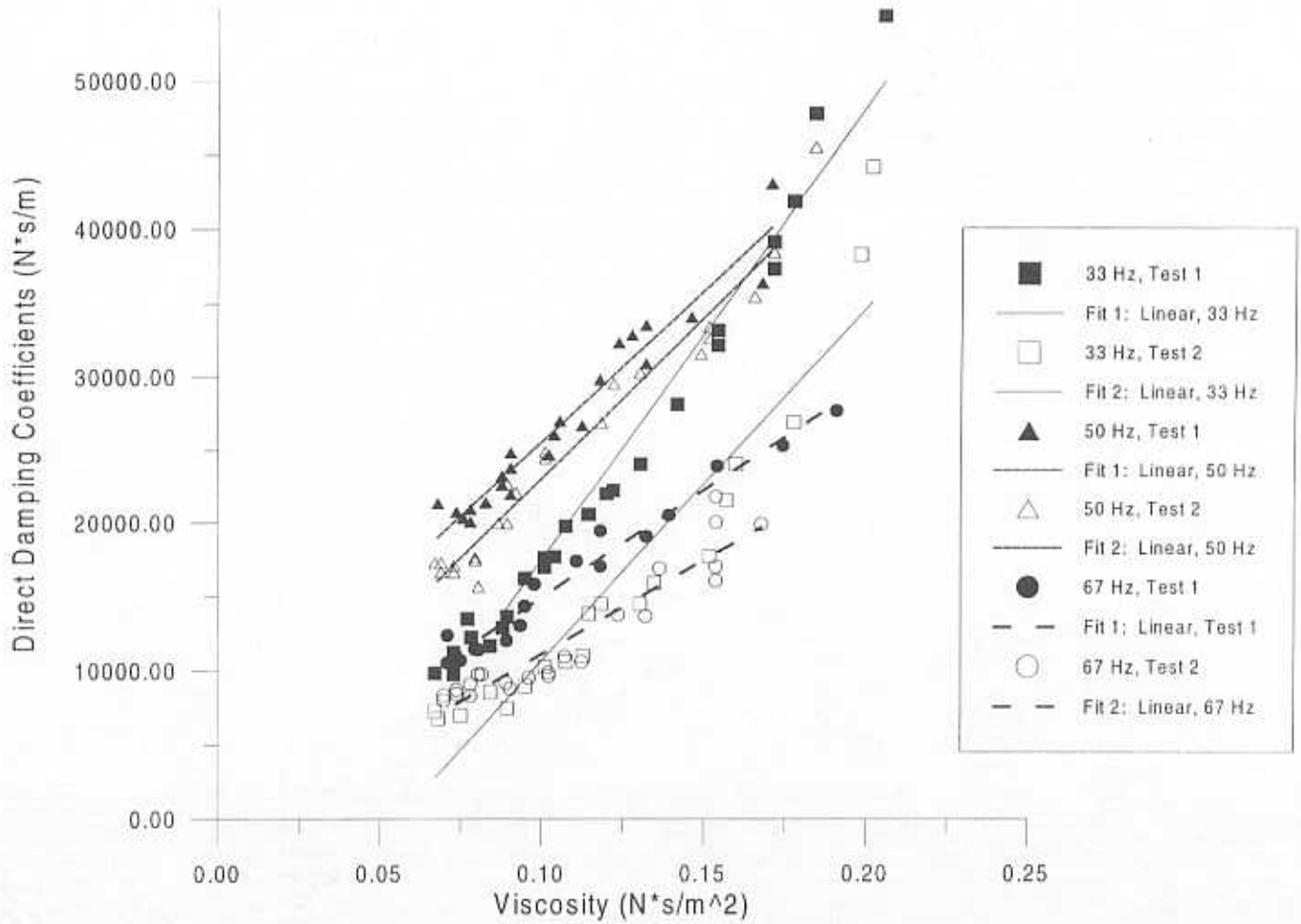

Figure 22.
Effect of Viscosity on Direct Damping Coefficients
at Different Frequencies
(SAE 30 Oil @ 69 kPa)

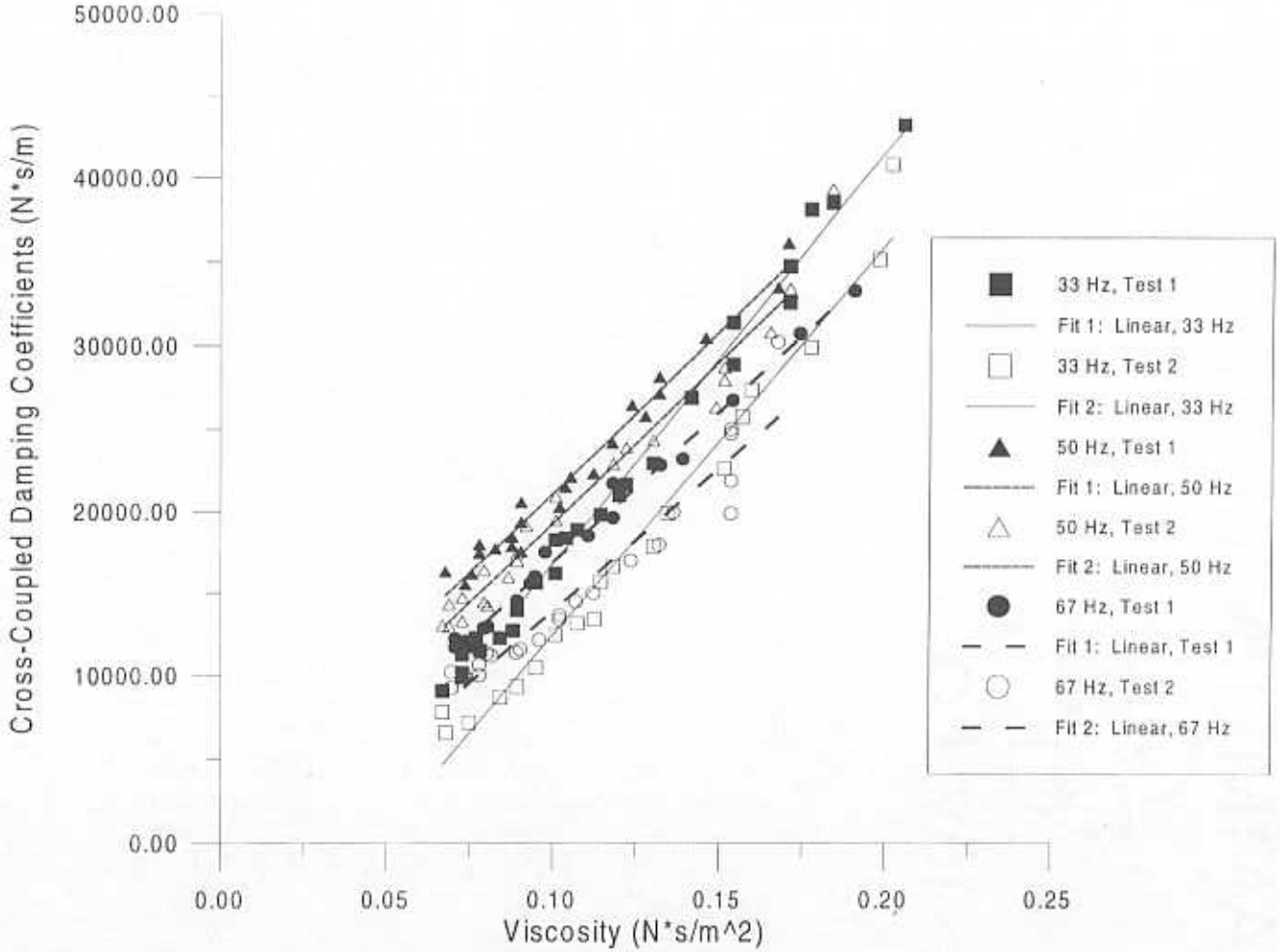

Figure 23.
Effect of Viscosity on Cross-Coupled Damping Coefficients at Different Frequencies (SAE 30 Oil @ 69 kPa)

their theoretical values (equation (5)). Figure 24 shows how at low viscosity values, the data that agrees the most with the theoretical π-film model is the data at 50 and 67 Hz. The results at 33 Hz, consisting of the greatest amount of gaseous cavitation, are half of their theoretical values for low values of viscosity. The radial forces obtained at 50 Hz are 25-50% larger than their calculated theoretical values. At low viscosities, the radial forces at 67 Hz are about 25% smaller than their theoretical values. Comparison of the experimental and theoretical tangential forces shows good correlation for the data obtained at 50 Hz. However, for most viscosity values, the tangential forces obtained at 33 and 67 Hz are about half of their theoretical values.

Tests for Increasing Pressure Supply

Figure 26 presents the effect of viscosity on the journal orbit radius for three supply pressures: 69, 138 and 207 kPa. Compared to the results in Figure 14, the orbit radius also decreases with increasing viscosity. However, for increases in supply pressure, the journal orbit radius shrinks.

The peak to peak dynamic pressures measured over a range of lubricant viscosities for three increasing supply pressures are shown in Figure 27a and b. The measurements do show increases in peak to peak dynamic pressures with increases in viscosity. When removing the effect of the orbit radius (Figures 28a and b), the peak to peak dynamic pressures increase with increases in supply pressure. Notice that the data at high pressures are very close to each other.

Figures 29 shows the effect of increasing lubricant supply pressure on the dynamic pressure distribution. These dynamic pressure measurements, selected at high lubricant viscosities, increase with increases in lubricant supply pressure. Comparison of these results to the ones obtained by Zeidan and Vance (*1990*) indicate that there is no cavitation present at high supply pressures, since both the "positive" and "negative" portions of the pressure wave extend over π radians of a cycle of motion.

The effect of viscosity on the radial force for increasing supply pressures is shown in Figure 30. The radial force tends to increase linearly with oil viscosity. Although the data points show a decrease of the radial force for increases in supply pressure, the standard deviation of the peak-peak pressures indicates that there is no significant influence of the pressure supply on the radial force.

Figure 31 presents the effects of lubricant viscosity on the tangential force for increasing supply pressure. The results show the linear increase in the tangential damping forces with increases in viscosity. They also demonstrate how slightly higher damping forces can be obtained by increasing the supply pressure.

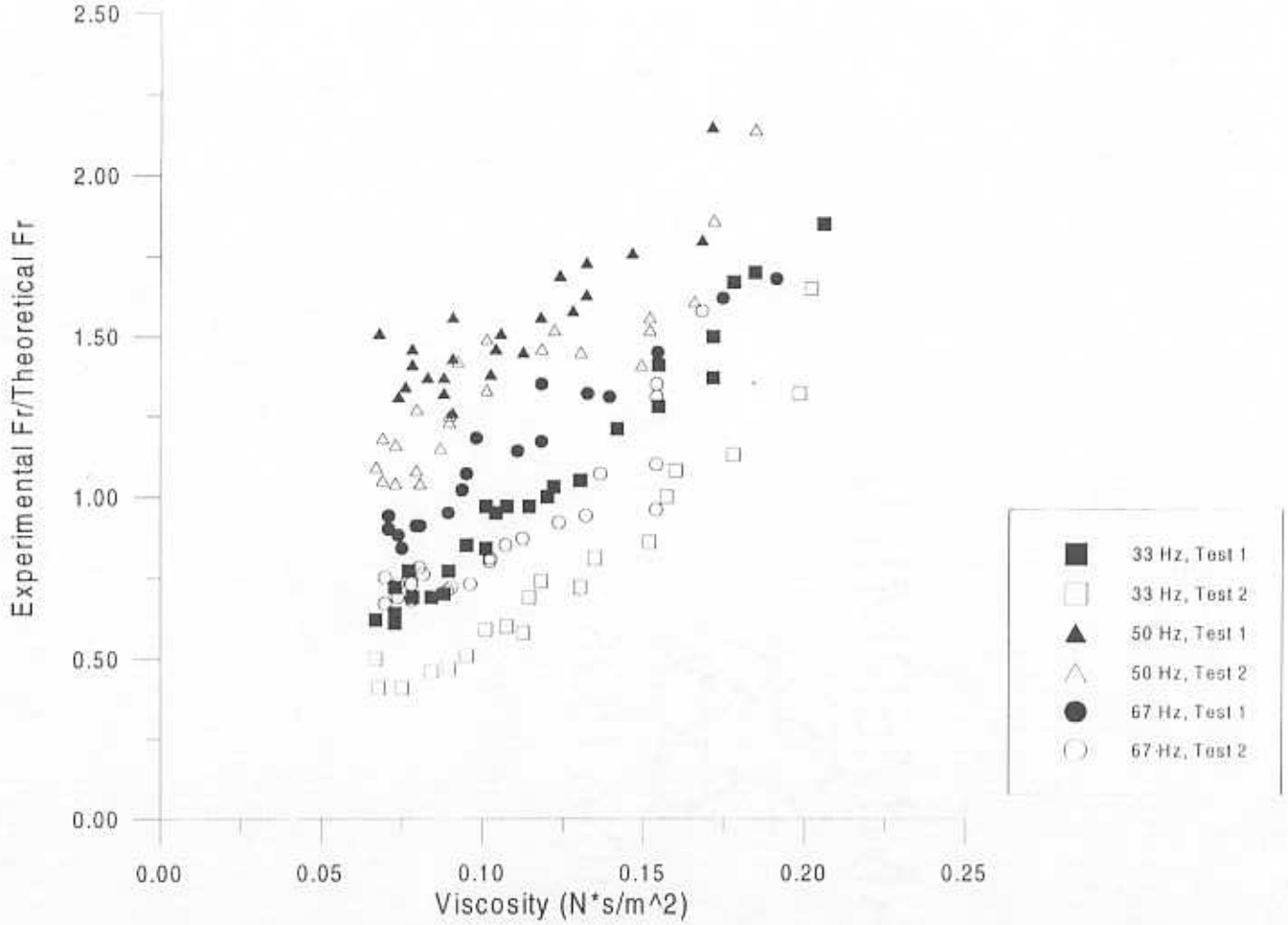

Figure 24.
Ratio of Experimental Radial Force to Short SFD Theoretical Radial Force
For Increasing Whirl Frequencies & Lubricant Viscosity
(SAE 30 Oil)

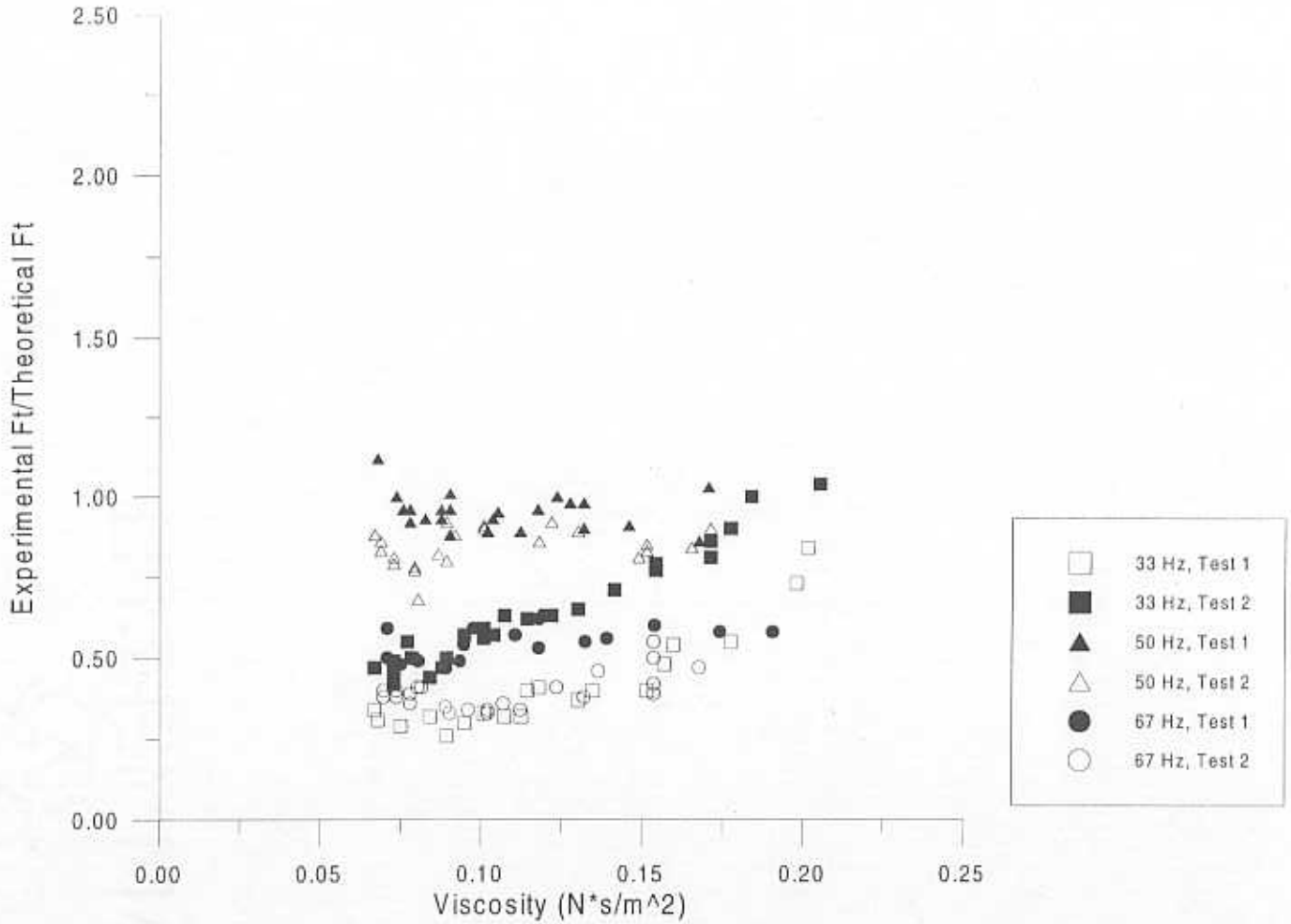

Figure 25.
Ratio of Experimental Tangential Force to Short SFD Theoretical Tangential Force
For Increasing Whirl Frequencies & Lubricant Viscosity
(SAE 30 Oil)

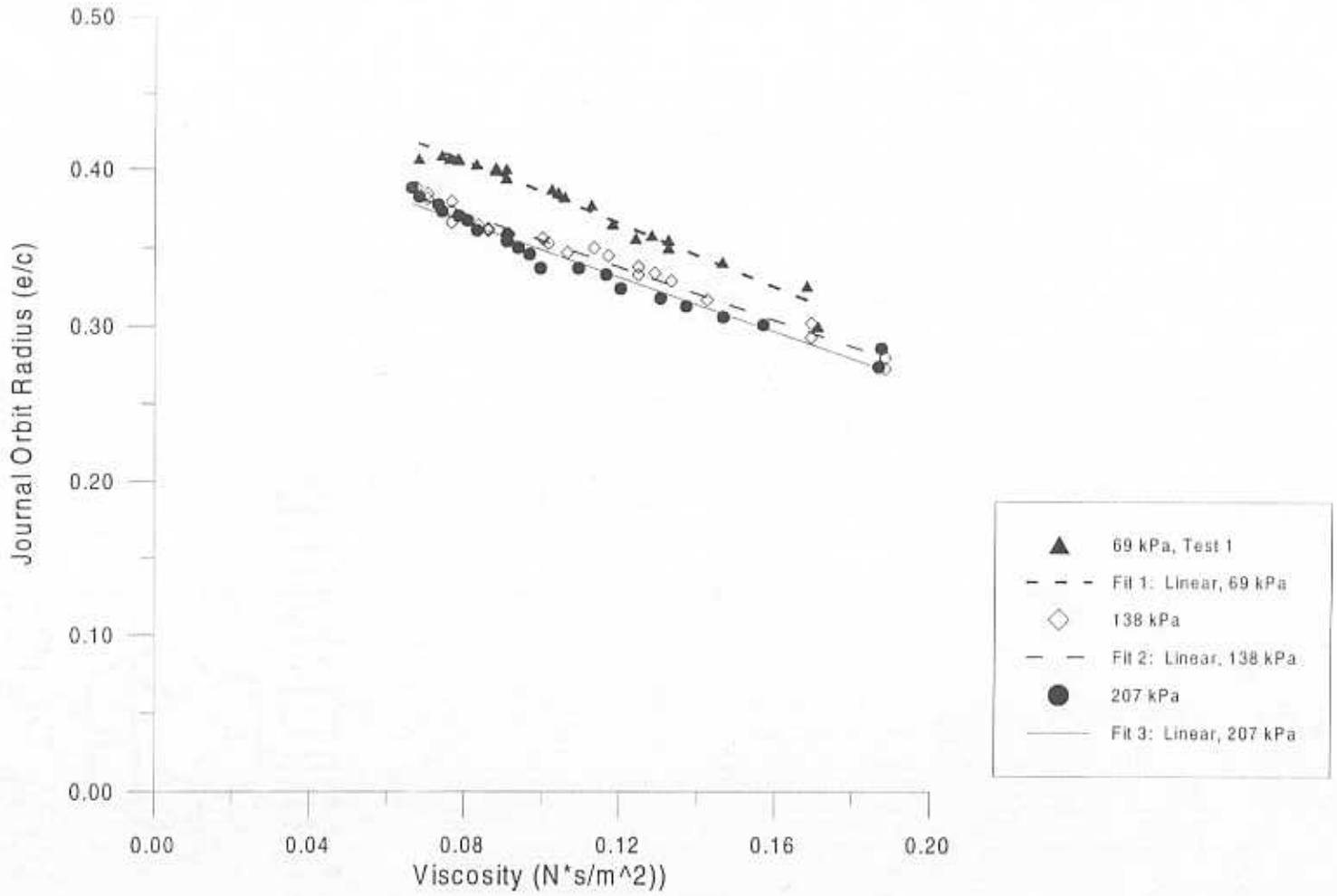

Figure 26.
Effect of Viscosity on Orbit Radius at w = 50 Hz
At Different Supply Pressures with SAE 30 Oil

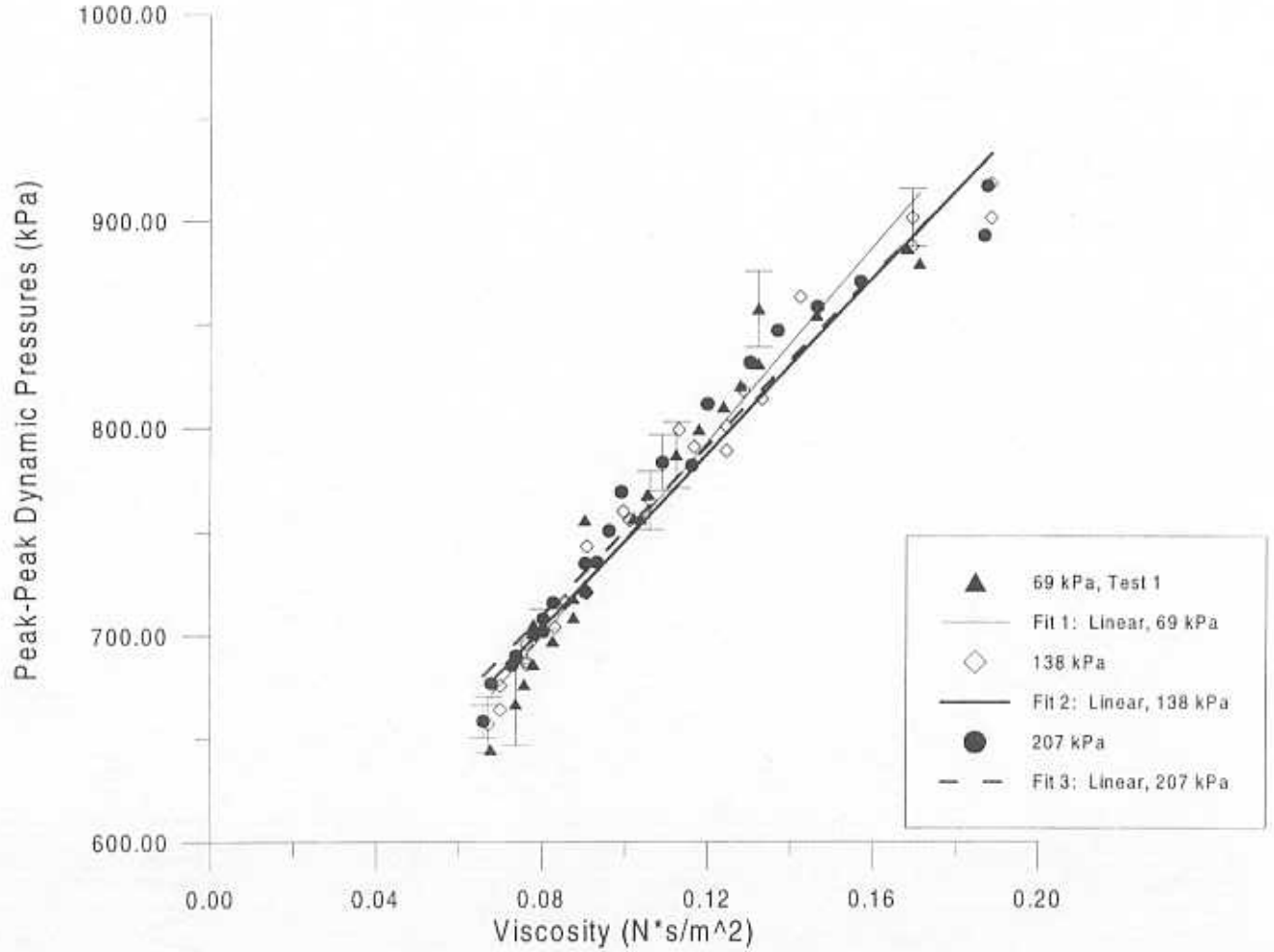

Figure 27a.
Effect of Viscosity on Peak-Peak Dynamic Pressures
at Different Supply Pressures
(SAE 30 Oil @ 50 Hz, Z1)

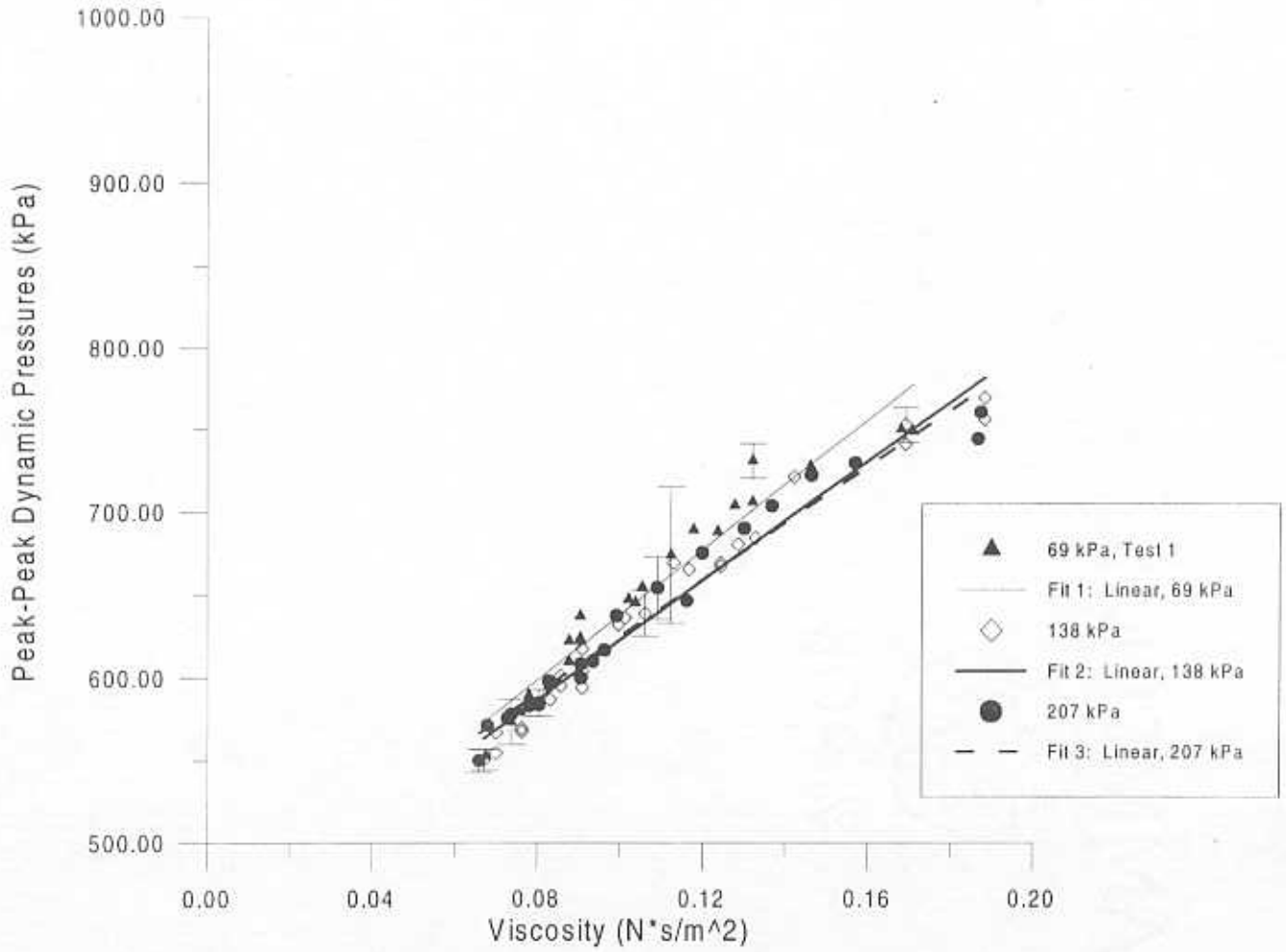

Figure 27b.
Effect of Viscosity on Peak-Peak Dynamic Pressures
at Different Supply Pressures
(SAE 30 Oil @ 50 Hz, Z2)

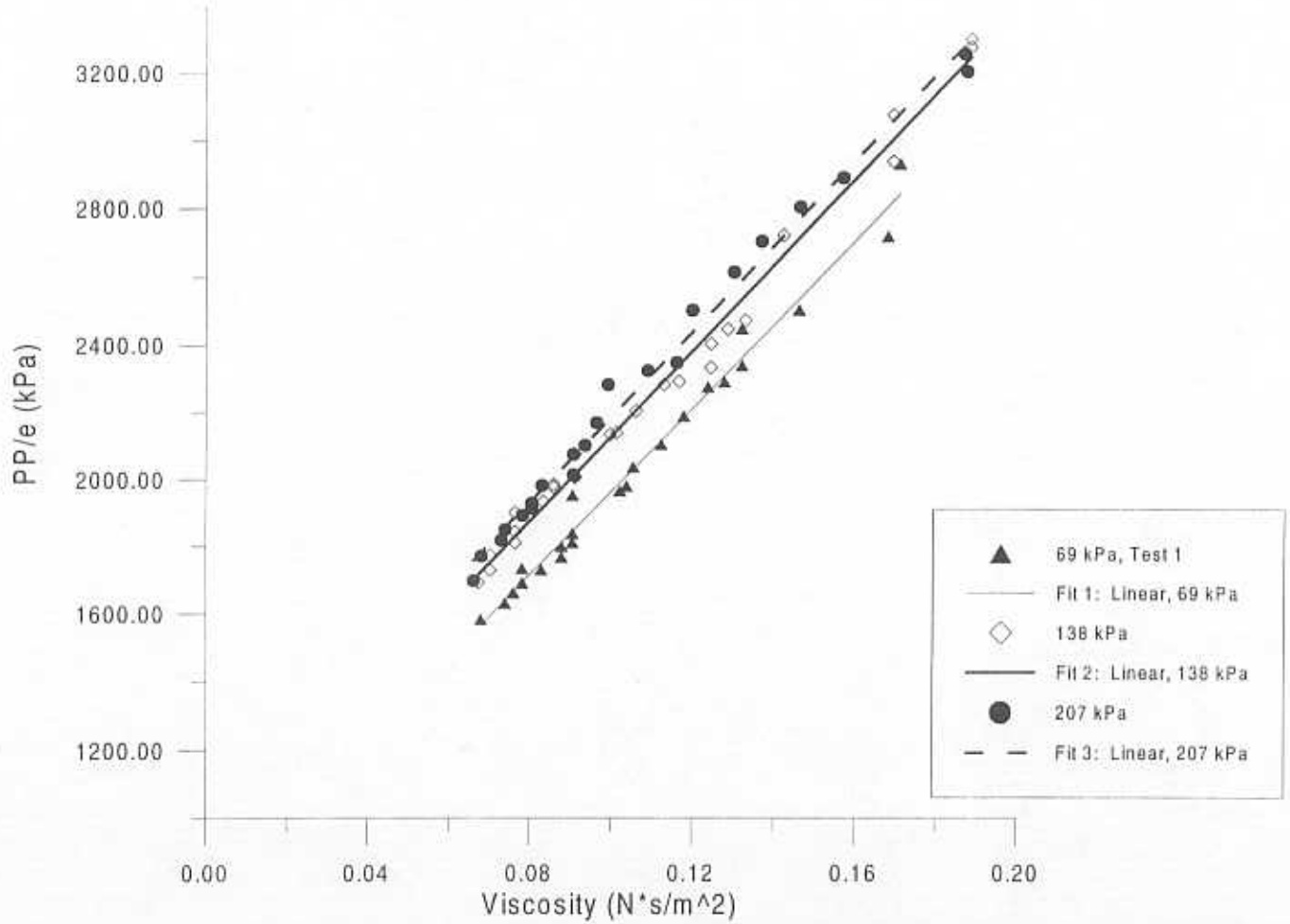

Figure 28a.
Effect of Viscosity on Peak-Peak Dynamic Pressures/Orbit Radius at Different Supply Pressures (SAE 30 Oil @ 50 Hz, Z1)

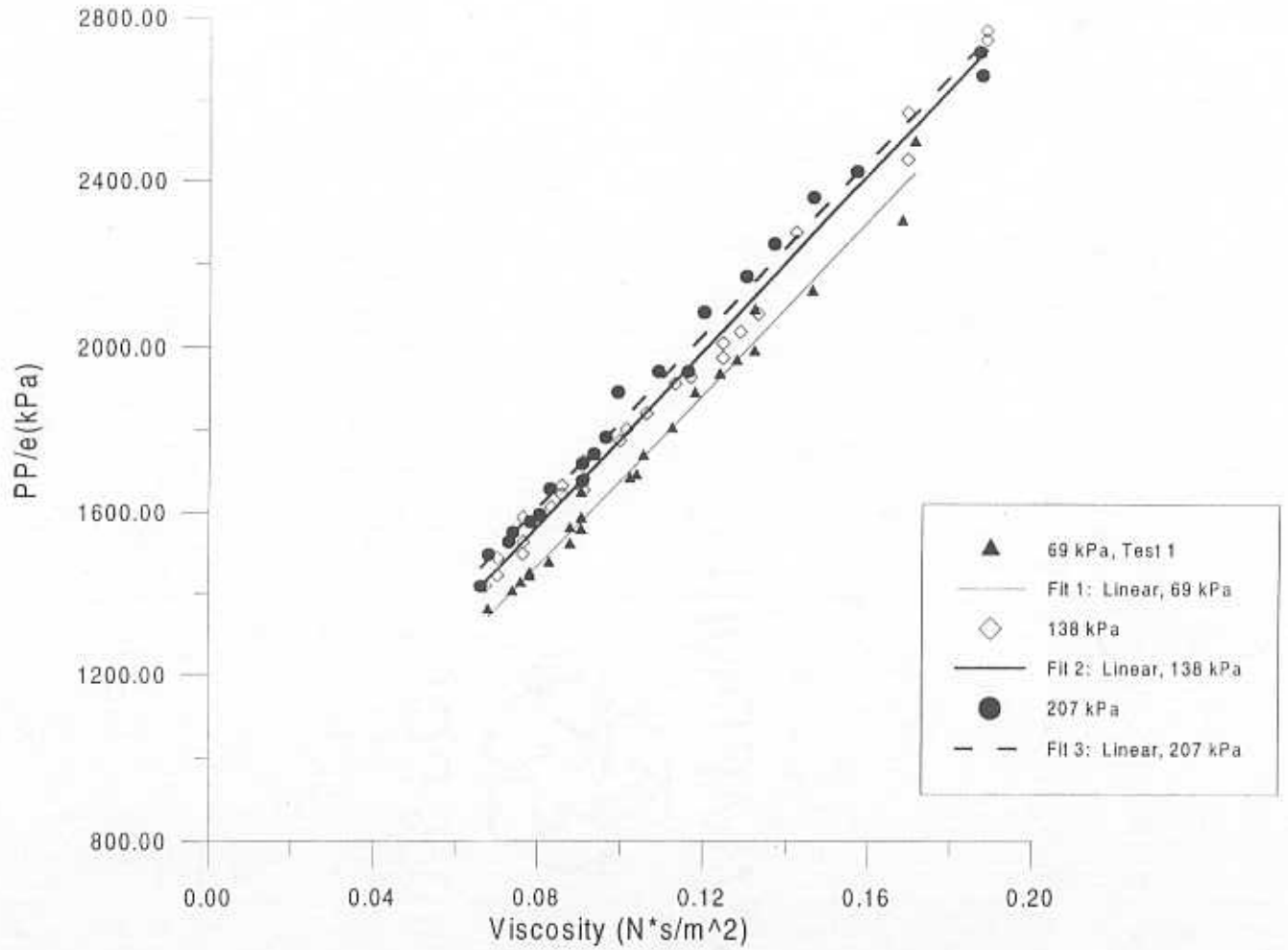

Figure 28b.
Effect of Viscosity on Peak-Peak Dynamic Pressures/Orbit Radius at Different Supply Pressures (SAE 30 Oil @ 50 Hz, Z2)

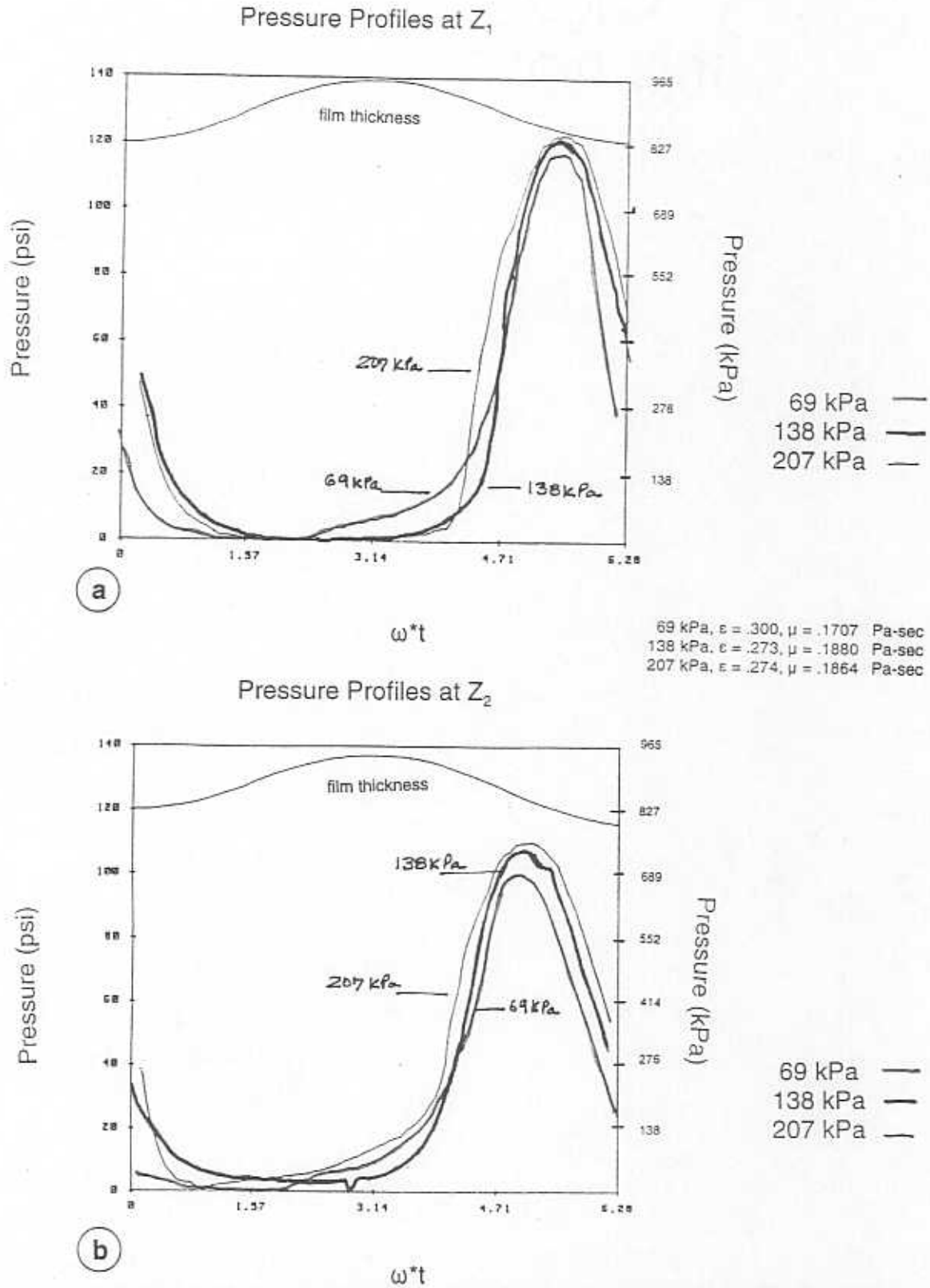

Figure 29 *Absolute Pressure vs. Time for Increasing Values of Supply Pressure At 50 Hz and at High Values of Viscosity*

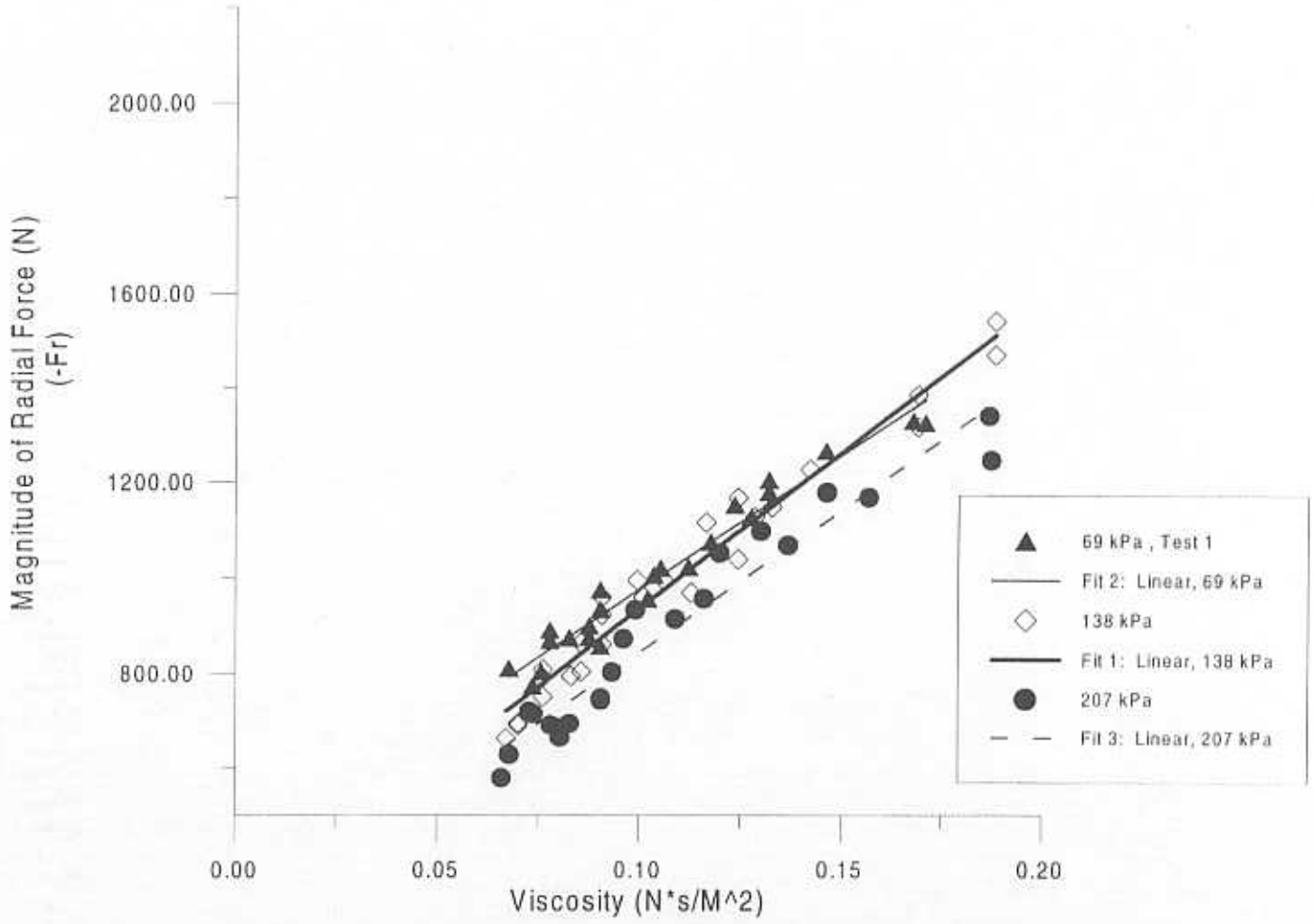

Figure 30.
Effect of Viscosity on Radial Force
For w = 50 Hz at Various Supply Pressures
(SAE 30 oil)

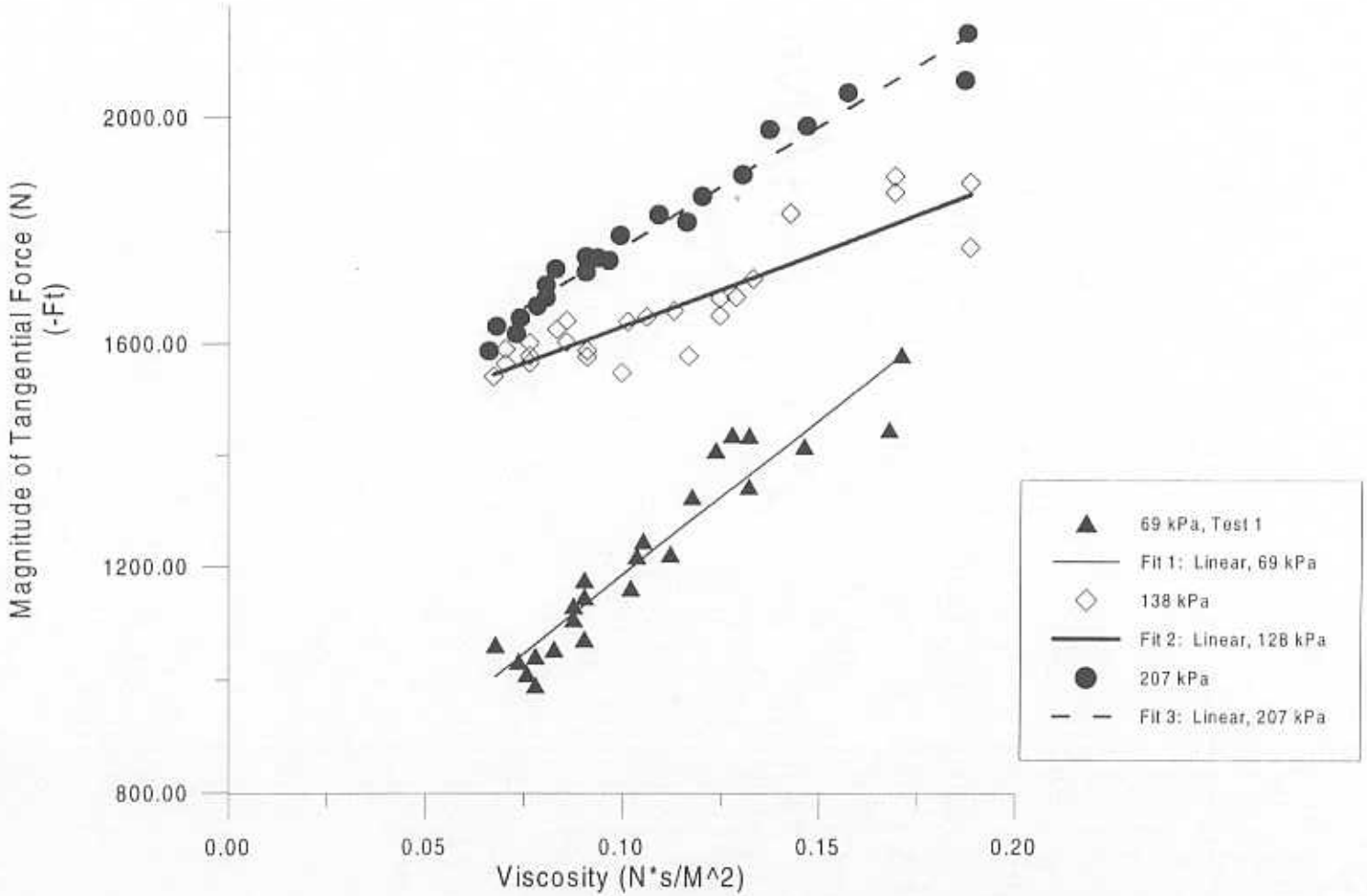

Figure 31.
Effect of Viscosity on Tangential Force
For w = 50 Hz at Various Supply Pressures
(SAE 30 oil)

The effect of viscosity on the direct damping coefficients (C_{rr}) for increases in supply pressure is shown in Figure 32. Like the tangential forces in Figure 31, the direct damping coefficients show a linear dependence on viscosity. Increasing the supply pressure also produces more damping, since cavitation is reduced.

For increases in supply pressure, the cross-coupled damping coefficients (C_{rt}) also show a linear dependence on the viscosity (Figure 33). The effect of increases in supply pressure, however, does not seem to be significant.

Figures 34 and 35 compare the experimentally obtained radial and tangential forces to their theoretical predictions for increasing supply pressures. At high supply pressures, Figure 34 presents the experimentally obtained radial force as almost twice as large as its theoretical prediction. At low viscosities (larger cavitated conditions, the experimental results agree more with the π-film theory. The tangential force (Figure 35) shows good agreement with theory at the lowest supply pressure 69 kPa. The results also show that increasing the supply pressure results in experimental tangential forces that are greater than their theoretical predictions (less cavitated cases). At high supply pressures and high values of lubricant viscosity, the tangential forces show better agreement with theory than at low values of viscosity.

Initially, an aerated lubricant was believed to be the originator of the deviations and discrepancies that appear in the data presented; however an unequal pressure distribution was identified at three different circumferential locations around the damper. This means that the journal is not centered. Thus,the experiments performed, based on a centered journal-theoretical model, will have to be repeated after the journal is centered. Only then can the meaning of the present results be verified and explained.

CONCLUSIONS

Dynamic pressure and film force measurements for a fully submerged open end squeeze film damper are presented for increasing whirl frequencies and supply pressures. The orbit radius varies inversely with fluid film viscosity and whirl frequency. These results show that the damper reduced the whirl amplitude of journal motion. The peak to peak pressures increase linearly with lubricant viscosity. The randomly computed error bars in the data indicate that the results at 50 and 67 Hz fall within the same range. The dynamic pressure distributions measured indicate increases in dynamic pressures with increases in whirl frequency. A combination of gaseous and vapor cavitation was observed throughout the different test conditions. As viscosity decreased, the extent of the cavitation zone increased. This was observed as a reduction in vapor cavitation and an increase in the gaseous cavitation zone. The radial and tangential forces

show a linear relationship with viscosity. They also increase with increases in whirl frequencies. The direct and cross-coupled damping coefficients behaved linearly with viscosity.

Increasing the pressure supply decreases the journal orbit radius and increases the peak to peak dynamic pressures. The magnitude of the peak to peak pressure distribution increases with increases in supply pressure. No cavitation was observed with increases in supply pressure. Increasing the pressure supply has a negligible effect on the radial force and cross-coupled damping coefficient, but increases the tangential force and the direct damping coefficient significantly.

The tests for varying frequency showed good agreement at 50 Hz with the experimental results of San Andres (*1995*). However, agreement of the present test results with the theoretical π-film model varied among the different whirl frequencies. For the tests with increasing supply pressure, comparison of the experimentally obtained radial and tangential forces to their theoretical predictions indicates that increasing the supply pressure results in underprediction of the forces. This is due to the fact that at greater supply pressures, cavitation is minimized.

The deviations and discrepancies that appear in the data presented originate from an off-centered journal. Different pressure distributions at three circumferential locations around the damper bearing verified this. In order to fully understand the present results, it is essential that the journal be centered and the experiments be repeated. The knowledge gained from these experiments will certainly serve as a guide to interpret and perhaps predict the results of future experiments with circular centered orbits.

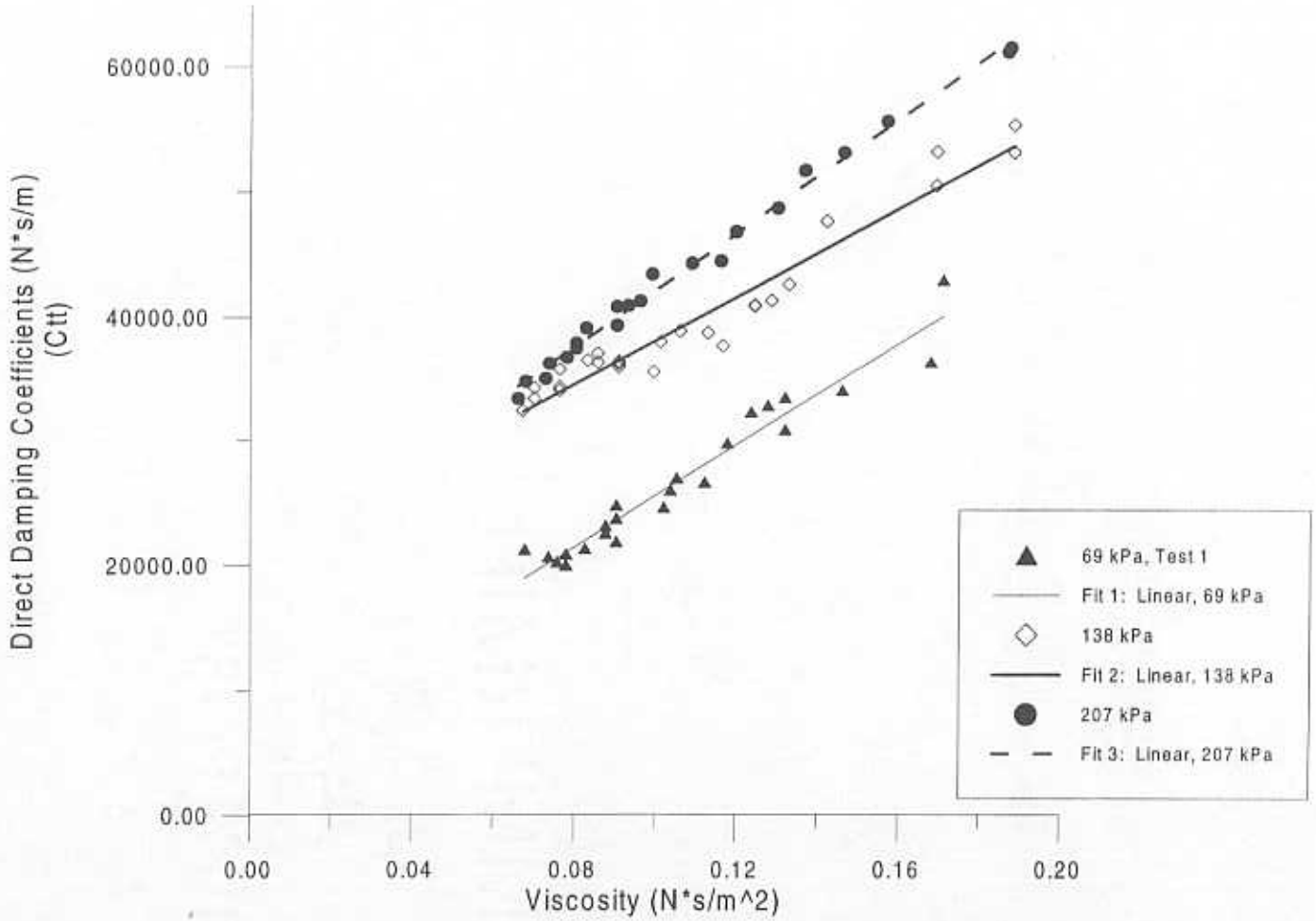

Figure 32.
Effect of Viscosity on Direct Damping Coefficients
at Different Supply Pressures
(SAE 30 Oil)

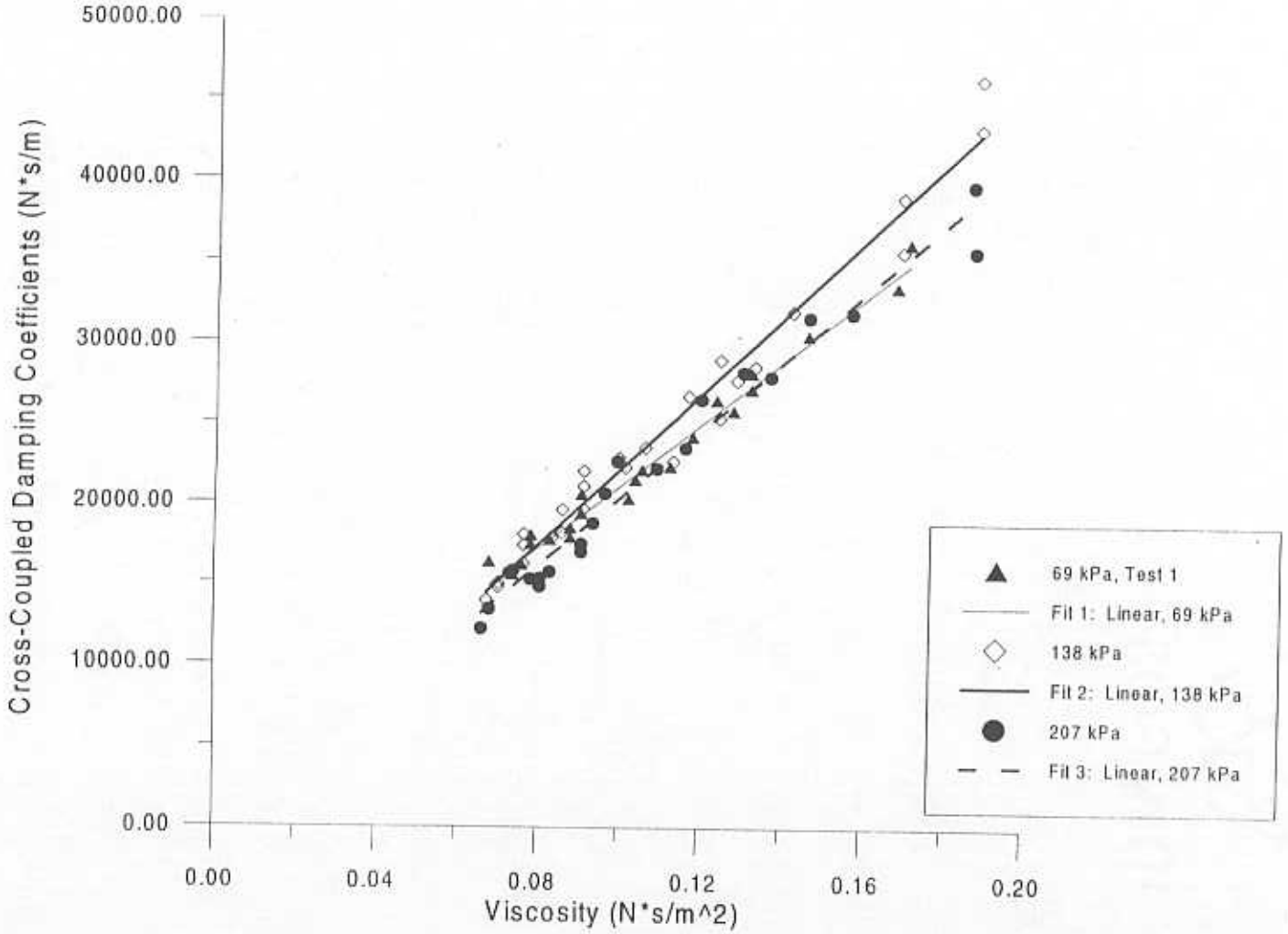

Figure 33

Effect of Viscosity on Cross-Coupled Damping Coefficients at Different Supply Pressures (SAE 30 Oil)

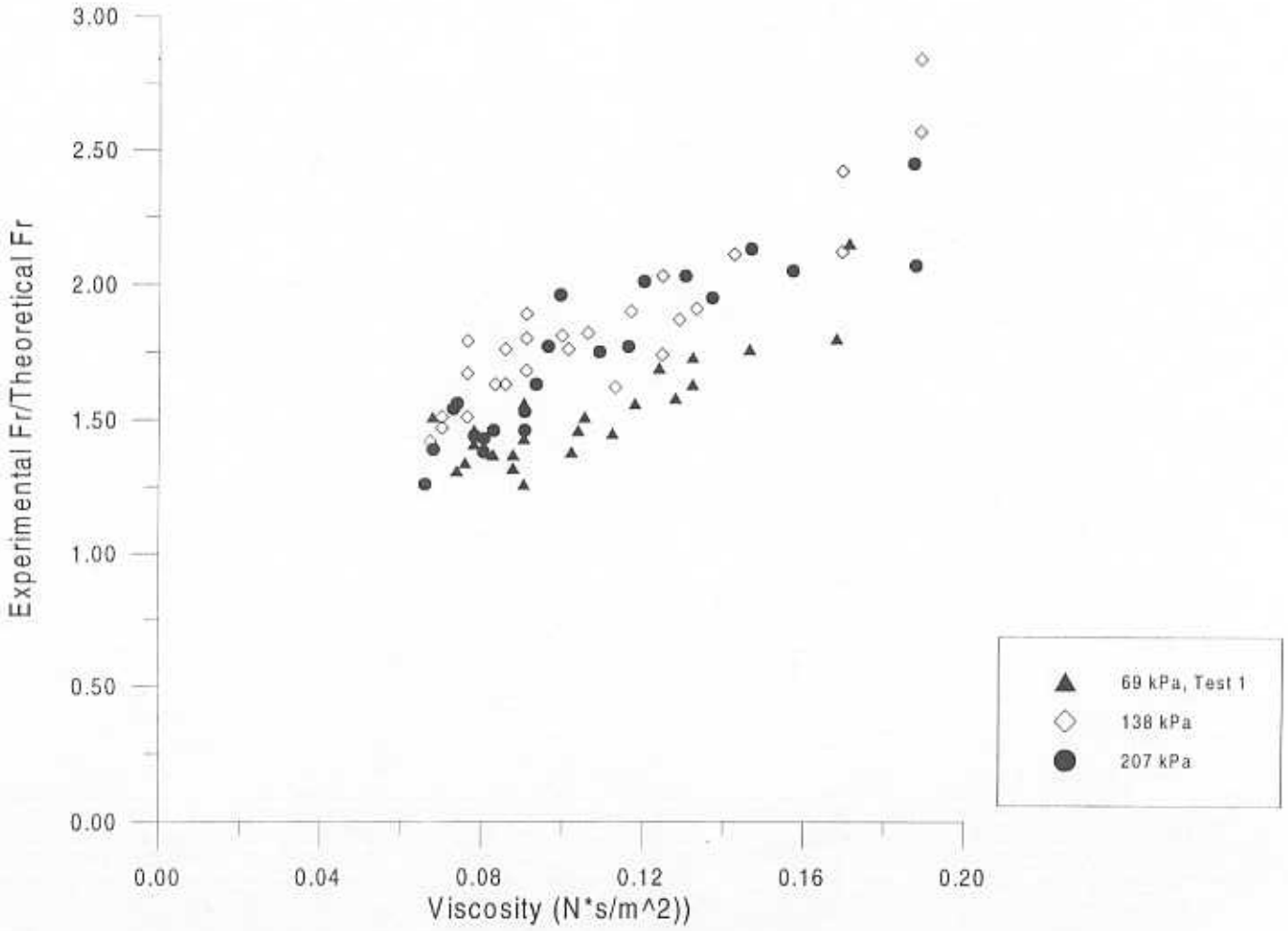

Figure 34.
Ratio of Experimental Radial Force to Short SFD Theoretical Radial Force At w = 50 Hz for Increasing Supply Pressures and Lubricant Viscosity (SAE 30 Oil)

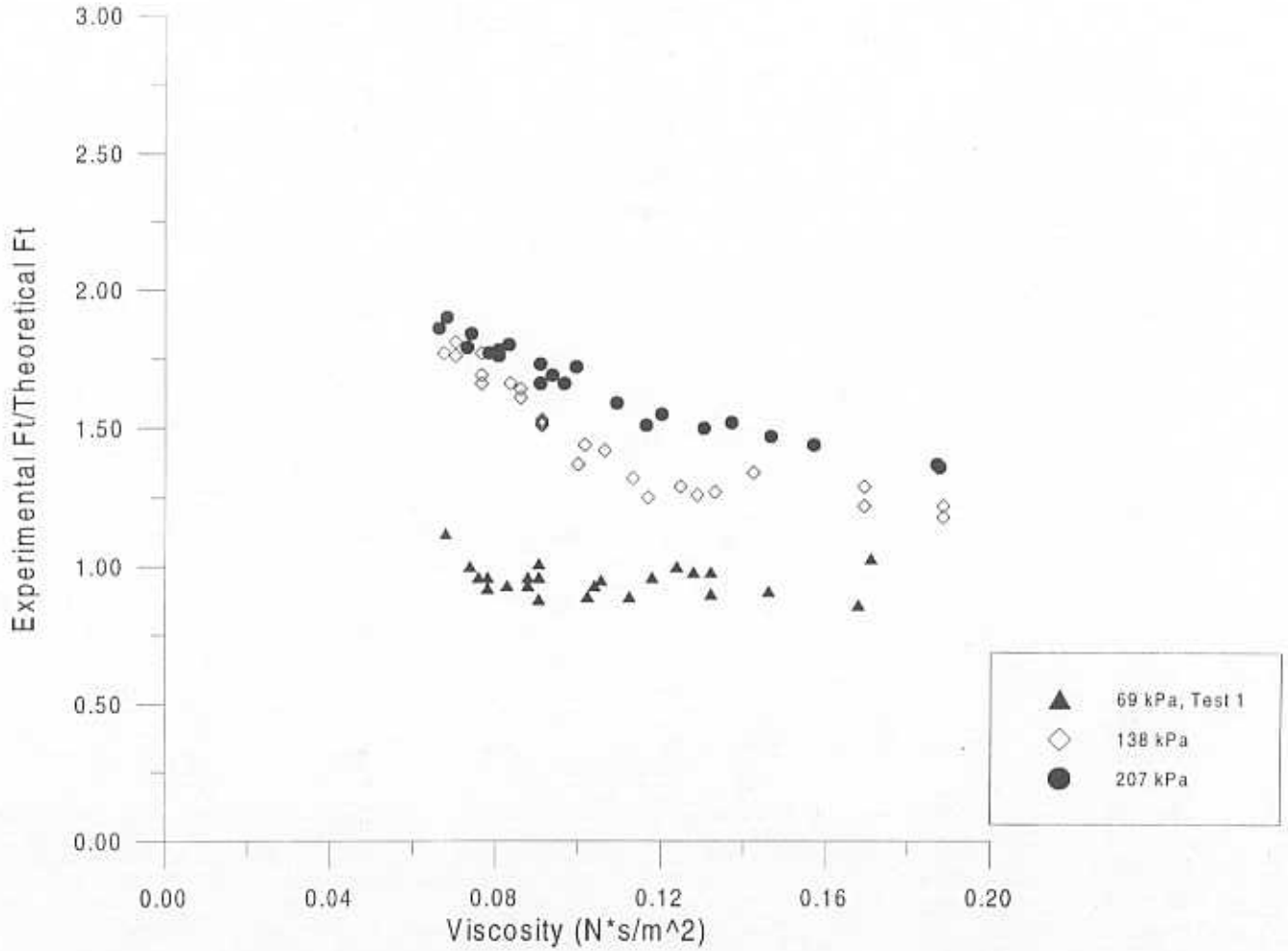

Figure 35.
Ratio of Experimental Tangential Force to Short SFD Theoretical Tangential Force At w = 50 Hz for Increasing Supply Pressures and Lubricant Viscosity (SAE 30 Oil)

REFERENCES

Arauz, G.L. and San Andres, L.A., 1993, "Effect of Circumferential Feeding Groove on the Dynamic Force Response of a Short Squeeze Film Damper," ASME Journal of Tribology, Vol. 116, pp. 369-367.

Childs, Dara, Turbomachinery Rotordynamics, John Wiley & Sons, Inc., 1993, pp. 214-221.

Feng, N.S., and Hahn, E.J., 1987, "Effects of Gas Entrainment on Squeeze Film Damper Performance," ASME Journal of Tribology, Vol. 109, pp. 149-154.

Hibner, D. H., and Bansal, P.N., 1979, "Effects of Fluid Compressibility on Viscous Damper Characteristics," Proceedings, Conference on the Stability and Dynamic Response of Rotors with Squeeze Film Bearings, U.S. Army Research Office, pp. 116-132.

Ramli, M.D., Roberts, J.B., and Ellis, J., 1987, "Estimation of Squeeze Film Dynamic Coefficients from Experimental Transient Data," ASME Jouranl of Tribology, Vol. 109 (1), pp 155-163.

Roberts, J.B., Holmes, R., and Mason, P.J., 1986, "Estimation of Squeeze Film Damping and Inertial Coefficient from Experimental Free-Decay Data," *Proc. of the Instn. of Mechanical Engineers*, Vol. 200, 2C, pp. 123-133.

Roberts, J.B., and, Ellis, J., 1989, "The Determination of Squeee Film Dynamic Coefficients from Transient Two-Dimensional Experimental Data, " ASME-STLE Joint Tribology Conference, October, Fort. Lauderdale, Florida.

Rouch, K.E., 1990, "Experimental Evaluation of Squeeze Film Damper Coefficients with Frequency Domain Techniques," ASLE Transactions, Vol. 33, 1, pp. 67-75.

San Andres, L.A., and Vance, J.M., 1986, "Effects of Fluid Inertia and Turbulence on the Force Coefficients for Squeeze Film Dampers," ASME Journal of Engineering for Gas and Turbines and Power, Vol. 108, pp. 332-339.

San Andres, L.A., and Vance, J.M., 1987a, "Experimental Measurement of the Dynamic Pressure Distribution in a Squeeze-Film Damper Executing Circular-Centered Orbits," *ASLE Transactions*, Vol. 30, No. 3, pp 373-383.

San Andres, L.A., and Vance, J.M., 1987b,"Effects of Fluid Inertia on Finite Length Squeeze-Film Dampers," ASLE Transactions, Vol. 30, No. 3, pp. 384-393.

San Andres, L.A., Meng, G., and Yoon, S., 1991a, "Dynamic Response of an Open End Squeeze Film Damper," ASME paper No. 91-GT-247.

San Andres, L.A., Meng, G., and Yoon, S., 1991b, "Dynamic Force Response of a Partially Sealed Squeeze Film Damper," ASME Mechanical Vibration and Design Conference, Miami, Fla., Vol. DE-35, *Rotating Machinery and Vehicle Dynamics*, pp. 251-256.

San Andres, L.A., 1991c, "Analysis of Short Squeeze Film Dampers with a Central Groove," ASME Paper No. 91-Trib-46.

San Andres, L.A., 1995, "Theoretical and Experimental Comparisons for Damping Coefficients of a Short Length Open-End Squeeze Film Damper," ASME95-9T-91, ASME Turbo Expo'95 Land, Sea & Air Conference, Houston, June 1995.

Sun, D.C., and Brewe, D.E., 1990, "A High Speed Photography Study of Cavitation in a Dynamically Loaded Journal Bearing," ASME Journal of Tribology...

Szeri, A., Raimondi. A.A., and, A. Giron Duarte, 1983, "Linear Force Coefficients for Squeeze Film Dampers," ASME Journal of Lubrication Technology, Vol. 105, pp. 326-334.

Tichy, J.A., and M. Modest, 1978, "Squeeze Film in Arbitrary Shaped Journal Bearings Subject to Oscillations," ASME Journal of Lubrication Technology , Vol. 100, pp. 323-330.

Tichy, J.A., 1984, "Measurement of Squeeze Film Bearing Forces Including the Effect of Fluid Inertia," *ASLE Transactions*, Vol. 28, pp. 520-526.

Vance, J.M., Rotordynamics of Turbomachinery, John Wiley, New York, 1988, pp 240, 245.

Zeidan, F. Y., and Vance, J.M., 1990, "Cavitation Regimes in Squeeze Film Dampers and Their Effect on the Pressure Distribution," *STLE Tribology Transactions*, Vol. 33, No. 3, pp. 447-453.

Walton, II, J.F. et al, 1987, "Experimental Observation of Cavitating Squeeze Film Dampers," ASME Journal of Tribology, Vol. 109, pp. 290-295.

White, D.C., 1970, *Squeeze Film Journal Bearings*, Ph.D. dissertation, Cambridge University.